REPORT DOCUMENTATION PAGE

Form Approved OMB NO. 0704-0188

1. REPORT DATE (DD-MM-YYYY)	2. REPORT TYPE	3. DATES COVERED (From - To)
19-05-2013	Final Report	25-Sep-2009 - 24-Sep-2013

4. TITLE AND SUBTITLE
Digital Control of Exchange Interaction in a Spin-based Silicon Quantum Computer

5a. CONTRACT NUMBER
W911NF-09-1-0498

5b. GRANT NUMBER

5c. PROGRAM ELEMENT NUMBER
611102

6. AUTHORS
Leonid P. Rokhinson, James C. Sturm

5d. PROJECT NUMBER

5e. TASK NUMBER

5f. WORK UNIT NUMBER

7. PERFORMING ORGANIZATION NAMES AND ADDRESSES
Indiana University - Purdue University Fort Wayn
Sponsored Programs Services
Young Hall, 302 Wood Street
West Lafayette, IN 47907 -2108

8. PERFORMING ORGANIZATION REPORT NUMBER

9. SPONSORING/MONITORING AGENCY NAME(S) AND ADDRESS(ES)
U.S. Army Research Office
P.O. Box 12211
Research Triangle Park, NC 27709-2211

10. SPONSOR/MONITOR'S ACRONYM(S)
ARO

11. SPONSOR/MONITOR'S REPORT NUMBER(S)
56447-PH-QC.6

12. DISTRIBUTION AVAILIBILITY STATEMENT
Approved for Public Release; Distribution Unlimited

13. SUPPLEMENTARY NOTES
The views, opinions and/or findings contained in this report are those of the author(s) and should not contrued as an official Department of the Army position, policy or decision, unless so designated by other documentation.

14. ABSTRACT
We propose to investigate dc and ac properties of single and double vertical Si quantum dots with 3D confinement. The dots constitute the main building blocks of a scalable “flying qubit” quantum computer architecture proposed earlier by the PIs. The major advantages of the proposed qubits are “digital” control of the exchange interaction for two-qubit operations, strong confinement and large energy spacing, and elimination of top gates for electron confinement, which, ideally, will leave only one operational gate per qubit. Reduction of the number of controlling

15. SUBJECT TERMS
silicon, quantum computing, quantyum dots, Majorana fermions

16. SECURITY CLASSIFICATION OF:			17. LIMITATION OF ABSTRACT	15. NUMBER OF PAGES	19a. NAME OF RESPONSIBLE PERSON
a. REPORT	b. ABSTRACT	c. THIS PAGE			Leonid Rokhinson
UU	UU	UU	UU		19b. TELEPHONE NUMBER 765-494-3014

Report Title

Digital Control of Exchange Interaction in a Spin-based Silicon Quantum Computer

ABSTRACT

We propose to investigate dc and ac properties of single and double vertical Si quantum dots with 3D confinement. The dots constitute the main building blocks of a scalable "flying qubit" quantum computer architecture proposed earlier by the PIs. The major advantages of the proposed qubits are "digital" control of the exchange interaction for two-qubit operations, strong confinement and large energy spacing, and elimination of top gates for electron confinement, which, ideally, will leave only one operational gate per qubit. Reduction of the number of controlling gates will allow arrangement of qubits into a 2D array, which simplifies error correction schemes and reduces correction overhead by an order of magnitude.

During the course of the project we also investigated a feasibility of building topologically protected and, thus, inherently fault-tolerant quantum bits. The idea of topologically protected quantum computer requires creation of excitations with non-Abelian statistics. Such excitation are not present in ordinary matter, but can be synthesized in hybrid semiconductor-superconductor structures.

Enter List of papers submitted or published that acknowledge ARO support from the start of the project to the date of this printing. List the papers, including journal references, in the following categories:

(a) Papers published in peer-reviewed journals (N/A for none)

Received		Paper
04/17/2013	2.00	Leonid P. Rokhinson, Xinyu Liu, Jacek K. Furdyna. The fractional a.c. Josephson effect in a semiconductor–superconductor nanowire as a signature of Majorana particles, Nature Physics, (09 2012): 0. doi: 10.1038/nphys2429
05/18/2013	4.00	Jiun-Yun Li, Chiao-Ti Huang, James C. Sturm. The effect of hydrogen on the surface segregation of phosphorus in epitaxially grown relaxed Si0.7Ge0.3 films by rapid thermal chemical vapor deposition, Applied Physics Letters, (10 2012): 0. doi: 10.1063/1.4757123
05/18/2013	5.00	Chiao-Ti Huang, Jiun-Yun Li, James C. Sturm. Implant Isolation of Silicon Two-Dimensional Electron Gases at 4.2 K, IEEE Electron Device Letters, (01 2013): 0. doi: 10.1109/LED.2012.2228160
TOTAL:	**3**	

Number of Papers published in peer-reviewed journals:

(b) Papers published in non-peer-reviewed journals (N/A for none)

Received		Paper
TOTAL:		

Number of Papers published in non peer-reviewed journals:

(c) Presentations

L.P. Rokhinson, "Observation of the fractional ac Josephson effect: the signature of Majorana particles" Workshop "Majorana Fermion Zero Modes in Solid-State Systems: Experiment and Theory", Kalvi Institute of Theoretical Physics, UCSB, December 2-14, 2012

L.P. Rokhinson, "Observation of the fractional ac Josephson effect: the signature of Majorana particles" Workshop "Spin-Related Phenomena in Mesoscopic Transport" Nordita, Stockholm, Sweden, September 16-22, 2012

L.P. Rokhinson, "Observation of the fractional ac Josephson effect: the signature of Majorana particles" International Conference on Physics of Semiconductors, Zurich, Switzerland, late news, July 3- Aug 3, 2012 (Late news submission promoted into the main program by organizes)

L.P. Rokhinson, "Observation of the fractional ac Josephson effect: the signature of Majorana particles" Workshop "Majorana Fermions in Condensed Matter", Lorentz Center, Leiden, Netherlands, July 2-6, 2012

L.P. Rokhinson, "Observation of the fractional ac Josephson effect: the signature of Majorana particles" Microsoft Station-Q meeting, June 22-24, 2012

C. T. Huang, J. Y. Li, and J. C. Sturm, "Very low electron density in undoped enhancement-mode Si/SiGe two-dimensional electron gases with thin SiGe cap layers," 223rd Meeting of the Electrochemical Society, Toronto, ON, Canada, May. 12 – 17, 2013.

J. Y. Li, C. T. Huang, L. P. Rokhinson, and J. C. Sturm, "Extremely low electron density in a modulation-doped Si/SiGe 2DEG by effective Schottky gating," 222nd Meeting of the Electrochemical Society, Honolulu, HI, Oct. 7 – 12, 2012.

J. Y. Li, C. T. Huang, and J. C. Sturm, "Extremely sharp phosphorus turn-off slope and effect of hydrogen on phosphorus surface segregation in epitaxially-grown relaxed Si0.7Ge0.3 by RTCVD," International SiGe Technology and Device Meeting, Berkeley, CA, June 4 – 6, 2012.

C. T. Huang, J. Y. Li, and J. C. Sturm, "High breakdown voltage Schottky gating of doped Si/SiGe 2DEG system enabled by suppression of phosphorus surface segregation," International SiGe Technology and Device Meeting, Berkeley, CA, June 4 – 6, 2012.

J. Y. Li, C. T. Huang, L. Rokhinson, J. A. Ohlhausen, M. Malcolm, and J. C. Sturm, "High quality two-dimensional electron gases (2DEGs) in isotopically-enriched strained Si," 2012 APS March Meeting Session X29, Boston, MA, Feb. 27 – Mar. 2, 2012.

J. Y. Li, K. S. Chou, C. T. Huang, J. C. Sturm, and L. P. Rokhinson, "High quality two-dimensional electron gases (2DEGs) in modulation-doped and enhancement-mode Si/SiGe heterostructures," 2011 PCCM Symposium: Quantum Control of Solid State Systems, Princeton, NJ, Nov. 3 – 5, 2011.

J. Y. Li, C. T. Huang, J. C. Sturm, and L. P. Rokhinson, "High quality two-dimensional electron system (2DES) in n-Type Si/SiGe modulation-doped heterostructures grown by RTCVD," 2011 International Workshop on Silicon Quantum Electronics, Denver, CO, August 14 ~ 15, 2011.

Number of Presentations: 12.00

Non Peer-Reviewed Conference Proceeding publications (other than abstracts):

Received Paper

TOTAL:

Number of Non Peer-Reviewed Conference Proceeding publications (other than abstracts):

Peer-Reviewed Conference Proceeding publications (other than abstracts):

Received		Paper
04/17/2013	1.00	Jiun-Yun Li, James C. Sturm, Chiao-Ti Huang. High Breakdown Voltage Schottky Gating of Doped Si/SiGe 2DEG Systems Enabled by Suppression of Phosphorus Surface Segregation, 2012 International Silicon-Germanium Technology and Device Meeting (ISTDM). 2012/06/04 00:00:00, Berkeley, CA, USA. : ,
04/17/2013	3.00	J. Y. Li, C. T. Huang, L. P. Rokhinson, J. C. Sturm. Extremely Low Electron Density in a Modulation-Doped Si/SiGe Two-DimensionalElectron Gases by Effective Schottky Gating, ECS Electrochemical Energy Summit PRiME. 2012/10/10 00:00:00, . : ,
TOTAL:	**2**	

Number of Peer-Reviewed Conference Proceeding publications (other than abstracts):

(d) Manuscripts

Received		Paper
TOTAL:		

Number of Manuscripts:

Books

Received		Paper
TOTAL:		

Patents Submitted

Patents Awarded

Awards

Graduate Students

NAME	PERCENT_SUPPORTED	Discipline
Sunanda Koduvayur	1.00	
Chiao-Ti Huang	1.00	
Jiun-Yun Li	0.50	
FTE Equivalent:	**2.50**	
Total Number:	**3**	

Names of Post Doctorates

NAME	PERCENT_SUPPORTED
FTE Equivalent:	
Total Number:	

Names of Faculty Supported

NAME	PERCENT_SUPPORTED	National Academy Member
Leonid Rokhinson	0.08	
James C. Sturm	0.08	
FTE Equivalent:	**0.16**	
Total Number:	**2**	

Names of Under Graduate students supported

NAME	PERCENT_SUPPORTED	Discipline
Kevin S. Chou	1.00	Electrical Engineering
FTE Equivalent:	**1.00**	
Total Number:	**1**	

Student Metrics

This section only applies to graduating undergraduates supported by this agreement in this reporting period

The number of undergraduates funded by this agreement who graduated during this period:	1.00
The number of undergraduates funded by this agreement who graduated during this period with a degree in science, mathematics, engineering, or technology fields:.....	1.00
The number of undergraduates funded by your agreement who graduated during this period and will continue to pursue a graduate or Ph.D. degree in science, mathematics, engineering, or technology fields:.....	1.00
Number of graduating undergraduates who achieved a 3.5 GPA to 4.0 (4.0 max scale):	1.00
Number of graduating undergraduates funded by a DoD funded Center of Excellence grant for Education, Research and Engineering:	0.00
The number of undergraduates funded by your agreement who graduated during this period and intend to work for the Department of Defense	0.00
The number of undergraduates funded by your agreement who graduated during this period and will receive scholarships or fellowships for further studies in science, mathematics, engineering or technology fields:	1.00

Names of Personnel receiving masters degrees

NAME
Jiun-Yun Li
Chiao-Ti Huang
Total Number: 2

Names of personnel receiving PHDs

NAME
Sunanda Koduvayur
Jiun-Yun Li
Total Number: 2

Names of other research staff

NAME	PERCENT_SUPPORTED
FTE Equivalent:	
Total Number:	

Sub Contractors (DD882)

Inventions (DD882)

Scientific Progress

See Attachment

Technology Transfer

1. Foreword

The main objective of the proposal was to develop a new type of a silicon-based qubit with reduced number of control gates, high fidelity exchange operations and long decoherence times. The proposed qubits are 3D-confined Si dots embedded into relaxed SiGe with epitaxial interfaces. The proposal required development of an entirely new growth technology of Si/SiGe heterostructures, new fabrication techniques and development of a new epitaxial re-growth technology. In the proposed budget we were over-optimistic and significantly underestimated the amount of the effort required to develop these technologies, both in terms of equipment and personnel. For example, after thorough analysis of the doping profile of CVD-grown heterostructures we had to completely rebuild a CVD gas handling system in order to separate phosphine from other processing gases and achieve the required quality of Si/SiGe growth. Nevertheless, we made technological breakthroughs and eliminated major technological bottlenecks toward development of 3D-confined Si qubits. The highlights of our achievements are:

i) Growth of very high mobility (>500,000 $cm^2/V{\cdot}s$) 2DEGs, near record mobility for CVD growth (and 100-fold mobility increase in our system);

ii) Growth of isotopically-enriched ^{28}Si modulation-doped heterostructures with ^{29}Si concentration below 800ppm and a record mobility for isotopically-eriched structures exceeding 500,000 $cm^2/V{\cdot}s$;

iii) Growth of the first enhancement-mode isotopically-enriched ^{28}Si 2DEGs with mobilities up to 300,000 $cm^2/V{\cdot}s$;

iv) Surface segregation of phosphorus, which makes Schottky gating difficult, was reduced to record low levels ($1.5{\cdot}10^{14}$ cm^{-3}) with extremely sharp interfaces (6 nm/dec). A new model was proposed to explain the effects of surface hydrogen on the segregation. Schottky gating was demonstrated in low electron density ($6 \cdot 10^{10}$ cm^{-2}) modulation-doped 2DEGs with extremely low gate leakage.

v) With phosphorus segregation under control we demonstrated the first high quality inverted modulation-doped Si 2DEGs with record mobility 470,000 $cm^2/V{\cdot}s$. This development will enable growth of symmetrical bi-layer quantum well structures as well as low density shallow 2DEGs.

vi) Development of a new process for lateral electrical isolation of 2DEG by ion implantation. The sheet resistance of the implanted regions can be as high as $1{\cdot}10^{13}$ Ω/□ at 4 K. Thermal stability up to 550 ^oC makes the technique compatible with most subsequent processing steps to fabricate silicon quantum devices.

Most of these results were presented as conference papers and not published yet in refereed journals. While a couple of manuscripts are under preparation we decided to include detailed description of the results in this report.

In parallel with the development of the Si technology we explored a possibility of an entirely different approach to quantum computing. Several theoretical works formulated a concept of a topological quantum computer, where non-Abelian statistics of quasiparticles results in an inherited fault tolerance, the premise being that such exotic matter can be created. We were the first to fabricate a system where Majorana fermions, particles believed to have non-Abelian statistics, can be realized. We provided the most convincing experimental evidence of their existence. These experiments are the first step toward development of a fault tolerant quantum computer.

2. Table of Contents

3. Statement of the problem studied

Solid state qubits based on spins in quantum dots have considerable promise due to clear path to scalability, long lifetime and slow dephasing of electron spins in semiconductors. The most advanced experiments were performed on GaAs quantum dots. The major disadvantage of GaAs is non-zero nuclear spin which limits spin dephasing time T_1 to 10-100 ns, unless nuclear bath is intentionally polarized or special sequence of pulses of magnetic fields is applied. However, there exist intrinsic difficulties to achieve nuclear polarization due to dipole-dipole spin interaction within and across the dot boundaries. At the same time, applying additional pulses is a complex endeavor even in one or two-qubit systems, and will create insurmountable challenges in systems scaled up to a large number of qubits. Use of Si, especially pure Si^{28}, eliminates hyperfine interactions entirely and is expected to bring T_1 and T^*_2 into ms range. The objective of ARO-supported project was to develop new technology to confine electrons in Si using epitaxial confinement and demonstrate high-fidelity electron transfer between quantum dots. To achieve that goal a novel growth technology of SiGe/Si heterostructures has been developed and 2D electron gases with exceptionally high mobility, enhanced gating response and isotopic purity have been demonstrated.

We also investigated a drastically different way to QC design – a topologically protected quantum computer (TQC) – which does not suffer from noise and decoherence problems of conventional QC designs. The idea of a TQC relies on the existence of particles with non-Abelian quantum statistics, meaning that the result of consecutive particles exchanges depends on the order of the exchanges in a multi-particle system. In such a computer qubit operations are braidings (exchanges) of non-Abelian particles which can be performed within the ground state of the system and, thus, immune to local sources of decoherence. In our work we designed a system which supports non-Abelian excitations, and detected a signature of the first non-Abelian particle - Majorana fermions. This discovery paves the way for the design and implementation of an inherently fault-tolerant TQC.

4. Summary of the most important results

A. High Mobility 2DEGs by Chemical Vapor Deposition

A.1 Introduction

The two-dimensional electron gas (2DEG) in semiconductors is a fundamental low-dimensional system [A1] for condensed matter physics. Important physics such as integral and fractional quantum Hall effects were discovered in high-quality 2DEGs [A2, A3]. Furthermore, practical applications such as modulation-doped field-effect transistor (MODFET) [A4] or quantum computation [A5] were also realized by utilizing a 2DEG. The most importance feature of a 2DEG is its high electron mobility by using the so-called modulation-doping technique to separate the supply impurities and electrons [A6]. A record high mobility of 3.5×10^7 cm^2/V-s was demonstrated in a GaAs 2DEG at T < 1 K [A7]. However, for silicon, which is probably the most important element among all semiconductors, 2DEG had not been observed until Abstreiter's experiment in 1985, which showed that electrons can be confined in a strained Si layer sandwiched by relaxed SiGe layers [A8].

In the first Si 2DEG, the mobility was fairly low (~2000 cm^2/V-s) due to the high density of dislocation defects by a large lattice mismatch between Si and SiGe layers. With a thick graded $Si_{1-x}Ge_x$ layer ($0 < x < 0.3$) of several microns grown on a Si substrate followed by a relaxed $Si_{0.7}Ge_{0.3}$ layer, Ismail *et al*. demonstrated a much improved mobility of 535,000 cm^2/V-s [A9]. Even higher electron mobility of 800,000 cm^2/V-s was reported by Sugii *et al*. with a combination of MBE and solid phase epitaxy to provide an atomically flat interface, reducing the interface roughness scattering [A10]. On the other hand, Huang *et al*. recently demonstrated a record high mobility of 2×10^6 cm/V-s in their enhancement-mode device of undoped Si 2DEG by top gating and suggested the background impurity scattering as the limiting factor of electron transport [A11].

To summarize, the dominant scattering source in Si 2DEGs seemed very different for various structures and there is no systematic work on the effects of layer structure on electron transport properties in a Si 2DEG so far. In this section, the basic properties of a 2DEG will first be introduced briefly, followed by our experimental results of modulation-doped Si 2DEGs of different layer structures. We also show effective Schottky gating on a modulation-doped Si 2DEG to manipulate the electron density and mobility to identify the dominant scattering mechanism.

A.2 Characteristics of a Si 2DEG

A.2.1 Band Offset between Strained Si and Relaxed SiGe layers

For electron confinement, a tensile strained Si layer must be sandwiched by relaxed SiGe layers (Fig. A.1 (a)). A conduction band offset (ΔE_c) exists between a strained Si and a relaxed SiGe layers because the six degenerate valleys in the conduction band of strained Si layer split into two sub-sets of Δ_4 and Δ_2 (Fig. A.1(b)) [A13]. Due to the lower energy level of Δ_2 state than that of Δ_4 state, electrons are in Δ_2 states. In relaxed SiGe layers, the degeneracy of six is preserved and the conduction band offset ΔE_c between strained Si and relaxed SiGe represents the energy difference between the conduction band edge in SiGe and the energy level of Δ_2 in Si, which depends on the Ge fraction in the SiGe layer.

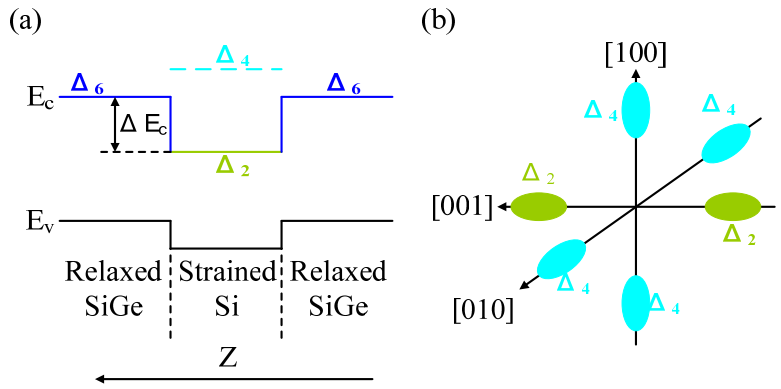

Fig. A.1 (a) Band diagram of a relaxed-SiGe/strained-Si/relaxed-SiGe heterostructure. The energy levels in the conduction band of strained Si are split into two states: Δ_2 and Δ_4; (b) under tensile strain, electrons reside in the two states of Δ_2 along (001) in Si with an in-plane effective mass of $m^* = 0.19\, m_0$ [A13].

A.2.2 Layer Structure and Epitaxial Growth

A typical layer structure of a Si 2DEG and the associated band energy diagram are shown in Fig. A.2. From the substrate to the surface, there are several epitaxial layers:

(i) $Si_{1-x}Ge_x$ graded buffer ($0 < x < 0.27$ for this work) + $Si_{0.73}Ge_{0.27}$ relaxed buffer,
(ii) strained Si quantum well (2DEG),
(iii) relaxed $Si_{0.73}Ge_{0.27}$ setback,
(iv) relaxed $Si_{0.73}Ge_{0.27}$ supply,
(v) relaxed $Si_{0.73}Ge_{0.27}$ cap
(vi) strained Si cap.

The basic functions of these layers in a Si 2DEG are described as follows: first, the $Si_{1-x}Ge_x$ graded layer ($0 < x < 0.27$) provides a buffer between the growth interface and the atop Si 2DEG layer. Due to the large lattice mismatch between Si and SiGe, the misfit dislocations exist at the growth interface and the threading dislocations punch through the 2DEG layer [A14]. With a slow grading rate of 10% Ge/μm, low-density misfit dislocation as low as 5×10^5 cm^{-2} could be achieved in a $Si_{1-x}Ge_x$ graded buffer ($0 < x < 0.3$) [A15]. Then a thick relaxed SiGe layer of constant Ge fraction is grown on top of the graded layer to offer a buffer of separating the dislocations and the atop strained Si layer for high electron mobility.

For (ii), a strained Si layer, where 2DEG resides, is grown between two relaxed $Si_{0.73}Ge_{0.27}$ layers, forming a quantum well for electron confinement. The thickness of this layer has to be complied with the critical thickness of strained Si on relaxed SiGe to prevent any further induced dislocations to reduce the electron mobility. A relaxed $Si_{0.73}Ge_{0.27}$ setback layer (iii) not only provides the required energy confinement for electrons in the Si QW layer, but also separates the supply layer of ionized impurities, leading to less impurity scattering. With the remote supply layer of n-type doping (iv), electrons can be "supplied" to the Si QW layer. Due to the separation of 2DEG and those ionized impurities in the supply layer, electron scattering can be reduced significantly, resulting in very high electron mobility [A6]. Due to the surface segregation of the n-type dopants in SiGe layers, a thick SiGe cap layer (v) has to be grown to avoid gate leakage due to a high doping concentration at surface for effectively gating quantum dot devices. Last, a Si cap layer offers a much more stable surface than SiGe, which is crucial for the subsequent processing steps.

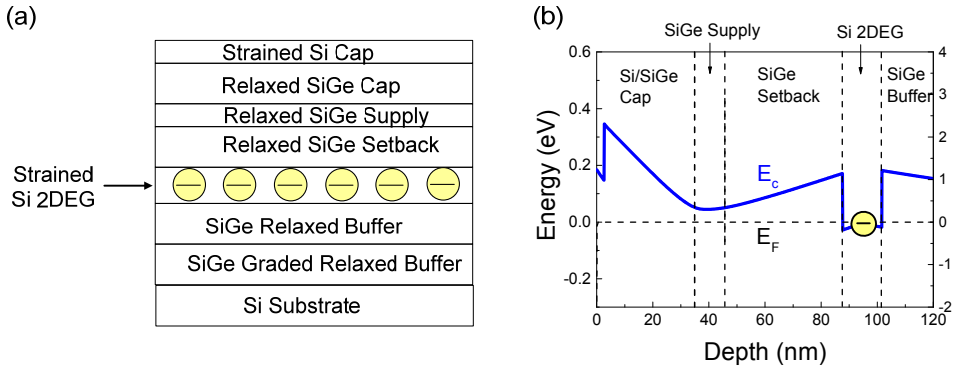

Fig. A.2 (a) Layer structure of a Si 2DEG and (b) the associated band diagram with a Ge fraction of 0.27 in a Si/SiGe heterostructure without gate bias.

In our work, the relaxed SiGe buffer layers were provided by Amberwave Inc. with a graded $Si_{1-x}Ge_x$ layer ($0 < x < 0.27$) of a grading rate of 10% Ge/μm grown on top of Si substrates followed by a $Si_{0.73}Ge_{0.27}$ buffer layer of 2 μm. Chemical mechanical polishing (CMP) was applied to reduce the surface roughness prior to the epitaxial growth. The wafers were cleaned by the following steps: 5 min in diluted HF (1%), 15 min in H_2SO_4: H_2O_2 (2.5:1), followed by 2 min in diluted HF (1%). Then the wafers were heated to 850 ^oC for 5 min in a hydrogen carrier at 6 torr to remove the residual oxide before the epitaxial growth started. Diluted SiH_4 and GeH_4 were used for the growth of Si and SiGe epitaxial layers. Diluted phosphine (100 ppm in hydrogen) was used as a doping gas for the growth of n-type SiGe supply layer. After baking, a SiGe buffer layer of 100 ~ 150 nm was grown at 575 ^oC, followed by a strained-Si layer (2DEG layer) of 6 ~ 30 nm at 625 ^oC, a SiGe setback layer of 10 ~ 70 nm at 575 ^oC, a n-type SiGe supply layer of 10 nm at 575 ^oC with a doping level between 10^{18} to 10^{19} cm^{-3}, a SiGe cap layer of 20 ~ 50 nm at 575 ^oC, and a Si cap layer of 2 nm at 625 ^oC.

The layer thicknesses, doping level, and Ge fraction were measured by SIMS. Ge, P, B, C, and O in a typical modulation-doped Si 2DEG (sample # 5737) are plotted versus depth in Fig. A.3. At the depth of 96 nm, a strained Si QW layer of 12 nm is sandwiched by the relaxed SiGe layers. The thickness of SiGe setback layer is 50 nm between the upper SiGe/Si interface and the position of the peak phosphorus level. The surface segregation of phosphorus was suppressed with a turn-off slope of 13 nm/decade in the SiGe cap layer, which was grown at 525 ^oC. At the re-growth interface of depth 255 nm, a spike of C and O indicates the incomplete removal of contaminants. Although baking at higher temperatures can be used for better cleaning of the growth interface, dislocations could be possibly created via the strain relaxation of the underlying graded $Si_{1-x}Ge_x$ layer. Thus, other approaches such as in-situ cleaning using HCl or HF, [A15] or a thick SiGe buffer layer which increases distance of remote scattering at the growth interface to 2DEG [A16] were suggested. In this work, the latter approach was.

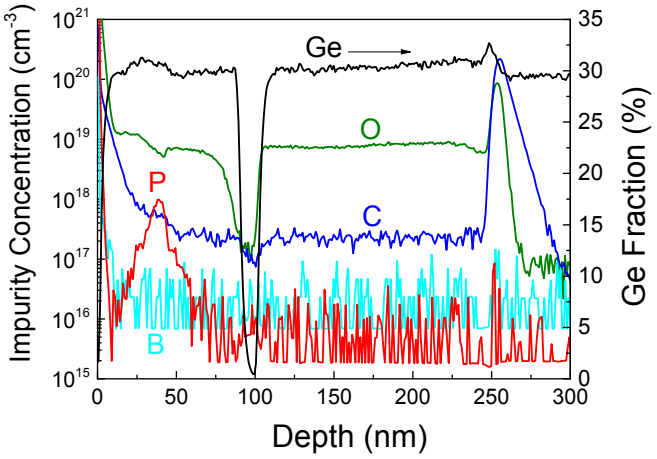

Fig. A.3 SIMS analysis of a typical Si 2DEG (sample #5737). Ge, P, B, C, and O were measured from the surface to below the growth interface at the depth of 255 nm.

After the growth, the wafers were mesa-etched in Hall bar geometry followed by AuSb deposition (1% Sb) and annealing at 450 ^{o}C in 10 minutes for electrical contacts. For gating experiments palladium was thermally evaporated to cover the entire Hall bar for Schottky gating. Low-temperature characterization was performed at 4 K or at 0.3 K in a ^{3}He system.

A.2.3 Electrostatics

In this section, we focus on the electrostatics of a Si 2DEG. By a simulator solving Poisson's and Schrödinger equations [A17], the energy diagram of conduction band in an ungated Si 2DEG at 4 K is plotted in Fig. A.4. Two boundary conditions were assumed for this band diagram. First, the Fermi level (E_F) is pinned at the midgap of Si surface layer due to the presence of many surface defects. The second boundary condition is that E_F is also pinned at the donor level (E_d) in the supply layer since the devices were measured at low temperatures. Electron density of 2DEG can be solved by the following equation [A18]

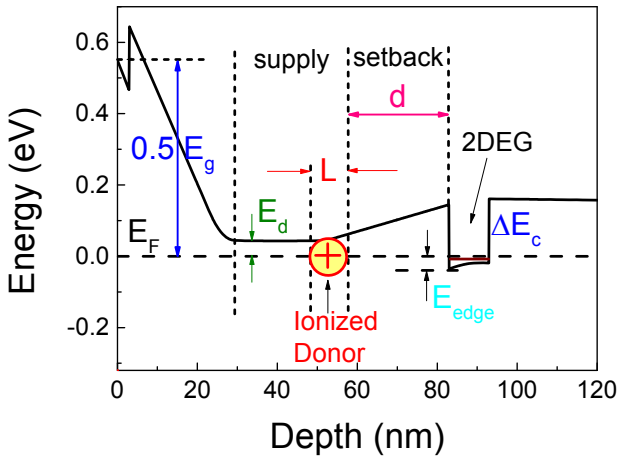

Fig. A.4 Conduction band diagram of a Si 2DEG at 4 K with two boundary conditions for the Fermi level (E_F) to be pinned at (i) the midgap of Si surface and (ii) the donor level.

$$\Delta E_C = E_{edge} + E_d + \frac{e^2 N_d L^2}{2\varepsilon\varepsilon_0} + \frac{e^2 n_{2D} d}{\varepsilon\varepsilon_0}, \quad \text{(A.1)}$$

where E_d is the energy difference between the donor level and the conduction band edge in the SiGe layer, E_{edge} is the energy difference between E_F and the conduction band edge at the upper SiGe/Si interface, and the last two terms represent the energy drop across the ionized impurity in the charged supply layer of length L and the neutral setback layer of length d.

Since the typical 2DEG density and the doping level are on the order of 10^{11} cm^{-2} and 10^{18} cm^{-3}, respectively, the required width L can be calculated by $N_d L = n_{2D}$ ~ 1 nm, which is much smaller than the thickness of the setback layer (20 ~ 70 nm). Therefore, the third term is usually ignored. Furthermore, E_{edge} of ~ hundreds μeV is fairly small compared to E_c (~ 180 meV for $Si_{0.7}Ge_{0.3}$ [A19]), to first order only the second and last terms are considered in the analysis. The electron density n_{2D} in the Si QW layer can be solved as

$$n_{2D} \approx \frac{\varepsilon\varepsilon_0}{e^2}\frac{\Delta E_C - E_d}{d}. \quad \text{(A.2)}$$

This shows the density at equilibrium (without external gating) can be manipulated by adjusting the conduction band offset (i.e. changing Ge fraction in the SiGe barrier) or the thickness of the setback SiGe layer. In this work, the Ge fraction is fixed at 0.27 and we focus on the effect of SiGe setback layer thickness on 2DEG characteristics.

A.2.4 Mobility Model

To analyze the scattering mechanisms in a Si 2DEG, we followed the procedures derived by Davies [A18]. For quantum dot applications, achieving a single electrons would require a low density in a 2DEG or a small dot area by a simple relation of 1 = n_{2D} × Area. With a QD of 30 nm × 30 nm, n_{2D} is as low as ~ 1 × 10^{11} cm^{-2}. Thus, we focus on the transport properties of 2DEG in the density below mid × 10^{11} cm^{-2}, where the impurity scattering has been suggested the dominant scattering mechanism [A20].

The strongest scattering at low temperatures in many 2DEG systems arises from ionized impurities such as n-type donors in the supply layer or throughout the entire material. The former is usually called remote impurity scattering and the latter is usually referred as background impurity scattering [A18, A20]. For remote impurity scattering, we assumed for simplicity that the supply layer is delta-doped with a two-dimensional density of N_{imp} ionized impurity, and located with a distance of d from the doping plane to the edge of Si QW layer. The resulting electron transport time can be expressed as

$$\frac{1}{\tau_{tr}} = \frac{\hbar N_{imp}}{32 m^* d^3 \sqrt{\pi n_{2D}^3}}, \quad \text{(A.3)}$$

where m^* is the effective mass of electron in the Si QW layer and the effects of degeneracy of two valley states and two spin states were included already. Then the mobility ($\mu = \frac{e\tau_{tr}}{m}$) is given by

$$\mu_{remote} = \frac{32 e d^3 \sqrt{\pi n_{2D}^3}}{\hbar N_{imp}}. \quad \text{(A.4)}$$

When n_{2D} increases, there is stronger electron screening [A18], so the mobility increases. As the distance between the plane of ionized impurities and 2DEG increases, electron scattering is weaker and the mobility is higher. On the other hand, as the number of ionized impurities is reduced, the remote scattering become weaker and the mobility will increase, too.

Ideally, in a 2DEG structure, the only doped region is the supply layer. However, in practice, in other layers, a minimum level of certain types of impurity exists, depending on the reactor history and growth conditions. The background impurities across the entire sample also scatter 2DEG with a predicted mobility as

$$\mu_{background} = \frac{2e\sqrt{n_{2D}}}{\sqrt{\pi}\hbar N_{background}}. \quad \text{(A.5)}$$

Similar to remote impurity scattering, as the electron density increases, background impurity scattering is reduced due to stronger electron screening. When the number of ionized background impurities is reduced, the scattering will be weaker.

The total mobility related to these two types of impurity can be written as

$$\frac{1}{\mu_{total}} = \frac{1}{\mu_{remote}} + \frac{1}{\mu_{background}}. \quad \text{(A.6)}$$

In the next section, we will show the importance of background scattering in a Si 2DEG grown. Then we present a much improved mobility by reducing the background impurity level in the CVD system at Princeton University.

Note the above model of 2DEG mobility was proposed with several assumptions made such as the delta doping in the supply layer. In practice, broadened n-type doping profiles in SiGe are induced by strong surface segregation, which might offset the predicted mobility by the above model. Furthermore, the abruptness of SiGe/Si/SiGe heterostructure may not be perfectly sharp, resulting in a perturbation on the quantum states in the Si QW layer. During the derivation for electron screening, many numerical approximations were made [A18]. This made the derivation easier, but is not of spectacular accuracy. As a result, in this work, we only use this theoretical model as a rough guide to help us understand the electron transport properties, but not for any precise numerical fitting or model comparison with our data.

A.3 Efforts toward High Mobility in Si 2DEGs

A.3.1 Effects of Phosphorus Background Impurity on 2DEG Mobility

In CVD systems, the background level of n-type dopants such as phosphorus or arsenic is usually very high due to memory effect [A21]. In Fig. A.5, SIMS data of a typical Si 2DEG (sample # 5144) are illustrated. The gas precursors for the epitaxial growth of this sample were SiH_2Cl_2 and diluted GeH_4 with diluted PH_3 as the n-type doping gas. At the depth of 40 nm, a phosphorus doped layer of 1.5×10^{18} cm^{-3} was grown. The phosphorus background levels in the Si and SiGe layers are 6×10^{17} cm^{-3} and 2×10^{17} cm^{-3}, respectively. Note below the growth interface at 250 nm, the phosphorus level in the relaxed buffer grown by Amberwave Inc. is below 10^{15} cm^{-3}, showing that the phosphorus levels in the epitaxial layers grown by our CVD are true, but not artifacts or detection limit from SIMS. By assuming $n_{2D} \sim 5 \times 10^{11}$ cm^{-2} and ignoring the remote impurity scattering, the electron mobility at a background impurity of 5×10^{17} cm^{-3} can be estimated by Eq. (A.5) as 5,000 cm^2/V-s, which is close to our experimental results of 3,000 ~ 8,000 cm^2/V-s. Thus, the first task to improve the 2DEG mobility is to lower the background impurity level in the epitaxial layers.

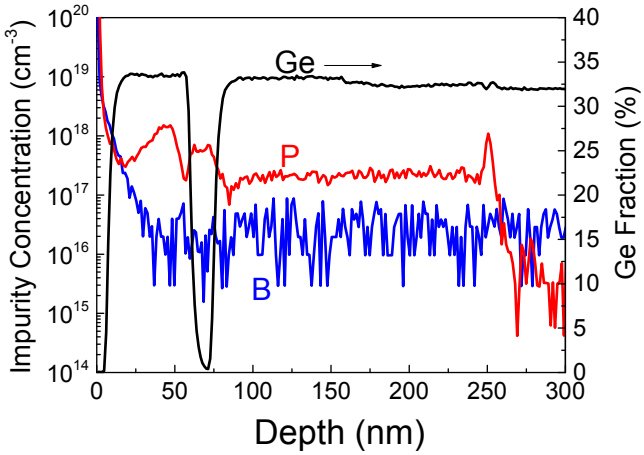

Fig. A.5 SIMS results of a Si 2DEG (sample #5144). The phosphorus background levels in Si and SiGe layers are 6 × 10^{17} cm^{-3} and 2 × 10^{17} cm^{-3}, respectively.

A.3.2 Reduction of Phosphorus Background Impurity

Low phosphorus background level has been suggested for a 2DEG of high mobility. In this section, we will introduce how we identified the sources for high background level of phosphorus in our CVD system followed by an approach to reduce the phosphorus level and our experimental results.

First, we evaluate the impacts of the potential sources for high phosphorus level such as the quartz tube and quartz wafer holder. Since Si wafers were often baked or annealed at high temperatures (~ 1000 °C) in our CVD system, the memory effect of absorbed phosphorus on the quartz walls might desorb and incorporate into the epitaxial films. To remove the coated phosphorus on the quartz wall and wafer stand, we used $HF:HNO_3:H_2O$ (1:4:6) to etch the deposited films on the quartz surface followed by DI water rinse. However, in a test 2DEG structure grown after the wet cleaning steps, phosphorus background level was rather high (~ 10^{17} cm^{-3}) and the mobility was still low (5,000 ~ 10,000 cm^2/V-s). Even with a brand new tube and wafer stand used for the growth of 2DEG devices, the identical results of high background level of phosphorus and low mobility were obtained. This suggests that the main source of phosphorus contamination would not be the tube and wafer stand.

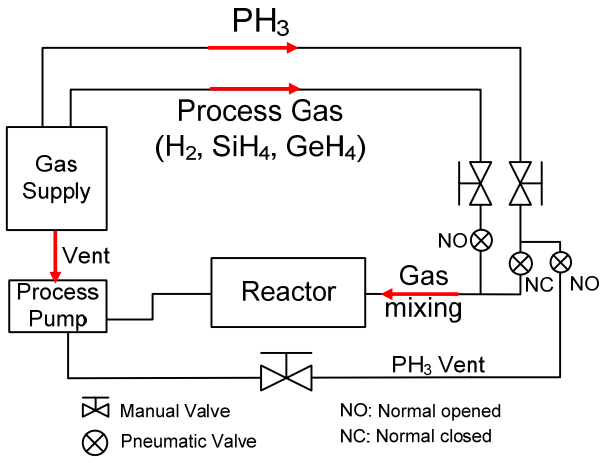

Fig. A.6 New gas supply system with a separation of process gases (H_2, SiH_4, GeH_4, etc.) and PH_3 to reduce the memory effect of phosphorus.

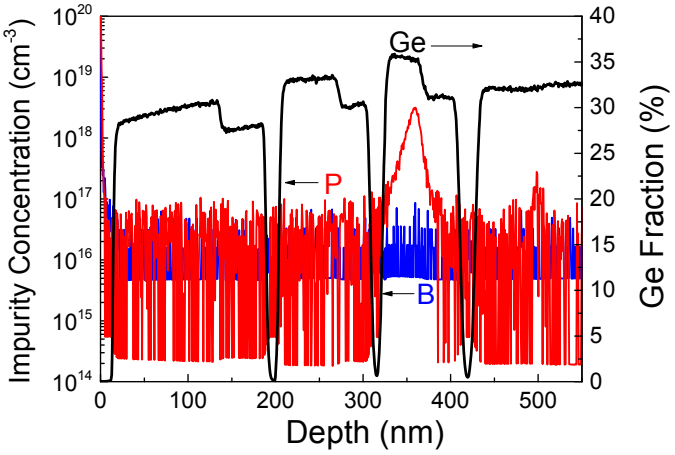

Fig. A.7 B, P, Ge profiles of a test structure of multiple Si and SiGe layers grown. Both B and P levels are down to the SIMS detection limits of 5×10^{15} and 3×10^{14} cm^{-3}, respectively except a phosphorus doped layer grown at the depth of 360 nm.

In addition to the quartz tube and stand, the manifold for gas mixing in the gas supply system could be another source for phosphorus contamination. To overcome this problem, we designed a gas separation system which isolates PH_3 and other gases (Fig. A.6). Phosphorus level is expected to be lower than that in the old panel because the cross-contamination is supposedly removed in this separation system. SIMS results of a test structure of undoped 2DEG structure (sample #5503) grown by this new gas panel supported our concept (Fig. A.7). Boron and phosphorus levels are as low as SIMS detection limit of 5×10^{15} cm^{-3} and below 10^{15} cm^{-3}. In this sample, a phosphorus doped layer was grown at the depth of 360 nm. The phosphorus levels before PH_3 turn-on and after PH_3 turn-off are identical, showing that the memory effect is insignificant by using a new panel equipped with the gas separation system.

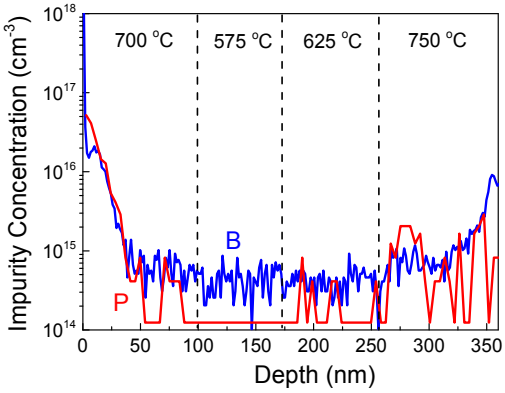

Fig. A.8 P and B profiles in Si layers grown at different temperatures (sample #5823).

A test sample was grown after more than 100 runs of 10 µm deposition in the reactor to confirm the negligible memory effect of phosphorus in the entire system. In this sample, only Si layers were grown at different temperatures with very thin SiGe layers as indicators for SIMS analysis (Fig. A.8). For phosphorus in the Si layer grown below 750 ^{o}C, its level is as low as the detection limit of 1.5×10^{14} cm^{-2}, which is three orders of magnitude lower than the level achieved with the old gas panel. Between 260

to 350 nm, the phosphorus level is slightly higher, probably since that layer was grown immediately after high temperature baking, when desorption of the absorbed phosphorus on the quartz wall was stronger, leading to higher incorporation into the films. For boron, although it is as low as the 3×10^{14} cm^{-3}, it is surprising that its level is slightly higher since boron precursor has never been used in the new gas panel. The low level of boron in the system could be a SIMS effect or the auto-doping from lightly boron-doped SiGe relaxed buffer substrates grown by Amerberwave Inc.

To estimate the effect of low background level of mid 10^{14} cm^{-3} on 2DEG mobility, we assumed 2DEG mobility is limited by the background impurity scattering and the mobility can be calculated as 3×10^{6} cm^2/V-s by Eq. (A.5), which is almost 10 times higher than the highest mobility reported in this work. Therefore, it is suggested that the mobility in 2DEGs grown by this new gas system is not limited by background impurity scattering, but probably remote impurity scattering. Further experimental results in the following sections confirm our conclusions.

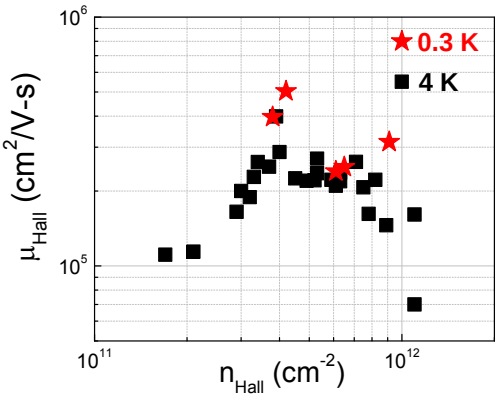

Fig. A.9 Hall mobility vs. electron density at low temperatures (4 K or 0.3 K). Highest mobility of 522,000 cm^2/V-s was measured at 0.3 K [A22]. Note each data point was taken from different samples with different layer structures.

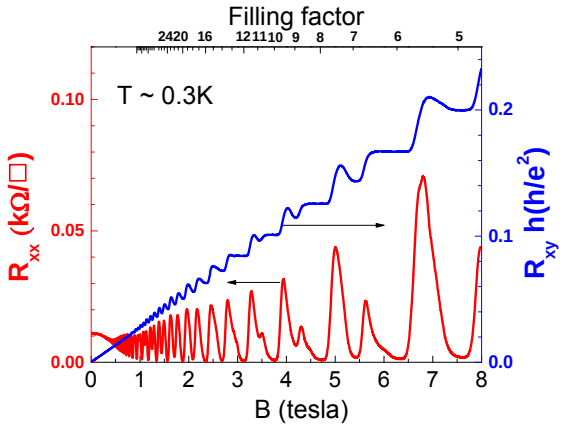

Fig. A.10 Longitudinal (R_{xx}) and transverse (R_{xy}) magneto-resistances vs. magnetic field at 0.3 K [A22].

Si 2DEGs of low background impurity were epitaxially grown by new gas panel and fabricated into Hall bar devices. Low-temperature (4 K and 0.3 K) electron density and mobility of Si 2DEGs with different layer structures were measured (Fig. A.9). The highest mobility was 522,000 cm^2/V-s [A22], ~ 100 times

higher than the level of samples grown by the old gas panel. The longitudinal (R_{xx}) and transverse (R_{xy}) magneto-resistances of sample #5446 were also measured at 0.3 K (Fig. A.10). Clear Shubnikov-de Haas oscillations in R_{xx} and quantum Hall plateaus in R_{xy} were observed, showing the high quality of this sample. The spin splitting and valley splitting occurred at 0.8 T and 3.5 T, respectively.

A.4 Effects of Layer Structure on 2DEG Mobility

A.4.1 SiGe Buffer Layer

Typically, a Si 2DEG structure was epitaxially grown on a Si (100) substrate either by MBE or CVD. We grew the epitaxial layers of a Si 2DEG on a virtual substrate which consists of a relaxed SiGe buffer layer on top of a graded SiGe layer on a Si substrate (provided by Amberwave Inc.). Prior to the growth, chemical mechanical polish was applied to reduce the surface roughness followed by a wet cleaning to remove the residual contaminants and native oxide on the polished relaxed SiGe surface. Then SiGe and Si epitaxial layers were grown by the new gas separation system and Hall bar devices were fabricated for electron transport measurement at low temperatures.

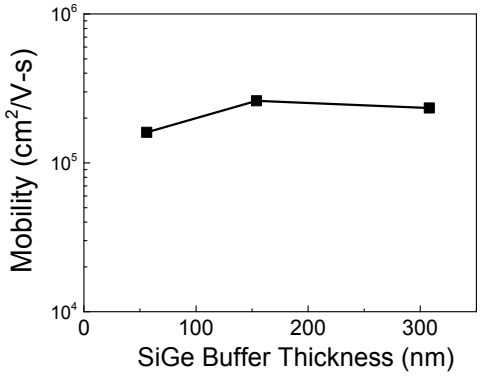

Fig. A.11 Electron Mobility at 4 K vs. SiGe buffer layer thickness.

As depicted in Fig. A.3, there were spikes of C and O in the growth interface due to the inefficient cleaning on the re-growth interface. Paul *et al*. suggested with a thick SiGe buffer layer on the SiGe virtual substrate, electron scattering from the bottom growth interface was much reduced [A16]. Thus, we grew test 2DEGs of three different thicknesses of SiGe buffer layer (75, 150, and 300 nm) and the rest of the layer structures was identical. Electron mobility measured at 4 K vs. SiGe buffer layer thickness is shown in Fig. A.11. The electron mobility was only slightly reduced for the device of 75-nm SiGe buffer layer, which followed the experiment results in [A16]. Although the density of C and O are high, how much they affect the electron transport (e.g. the ionization ratio and charge type) is not known yet. Since the SiGe buffer layer separate the growth interface and the 2DEG, the remote impurity scattering at this interface could be much reduced with a thicker SiGe buffer layer. By a saturation of electron mobility with SiGe buffer layer thickness > 150 nm, we think 2DEG transport is not limited by the remote impurity scattering from the growth interface and will not address the effect of C and O at the growth interface on 2DEG transport.

A.4.2 Si Quantum Well Layer

Since 2DEG is in a strained Si layer, several devices with different thicknesses of Si layer grown at 575 ^{o}C and 625 ^{o}C were made to investigate the effects of strained relaxation on 2DEG mobility. Electron mobility vs. Si QW thickness is shown in Fig. A.12. For 625 ^{o}C data, as the Si QW is thicker than 12 nm, the mobility drops significantly due to the dislocations created by strain relaxation of Si QW layer. This

thickness is very close to the reported critical thickness of strained Si on relaxed $Si_{0.73}Ge_{0.27}$ [A25]. For 575 °C, a similar trend was observed.

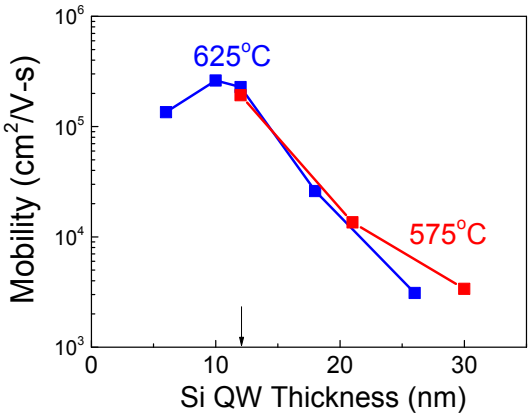

Fig. A.12 Mobility at 4 K vs. Si QW layer thickness grown at 575 °C and 625 °C. The arrow indicates the critical thickness of strained Si on relaxed $Si_{0.73}Ge_{0.27}$.

On the other hand, as Si QW is as thin as 6 nm, 2DEG mobility drops slightly, which could be attributed to the stronger scattering from the roughness at the upper SiGe/Si heterointerface [A26]. In a narrow QW, the spreading of electron wavefunction into the SiGe barrier layers becomes stronger, which might lead to stronger scattering from the remote impurity in the supply layer or alloy scattering in the SiGe barrier [A20]. Thus, when we discuss the ionized impurity scattering in the next section, the thickness of strained Si QW layer is controlled between 9 to 12 nm, to avoid the required complicated analysis to isolate the effects of different scattering mechanisms on 2DEG mobility.

A.4.3 SiGe Setback Layer

According to the analysis of electrostatics, the electron density in the 2DEG layer depends on the thickness of SiGe setback layer if enough carriers are provided from the supply layer. By adjusting the thickness of SiGe setback layer, the density can be modulated following Eq. (A.2). The experimental results of electron density vs. SiGe setback layer thickness is shown in Fig. A.13(a) with a theoretical calculation of Eq. (A.2). For quantum dot applications, a low electron density is preferred, so a thick setback layer is required. However, for a Si 2DEG of a thick setback layer, the control of top metal gates over the underlying 2DEG would be weaker. Thus, an optimized thickness of SiGe setback layer is usually used for quantum dot fabrication.

In Fig. A.13 (b), electron mobility is also plotted versus the setback layer thickness with a peak mobility at 30 nm. This could be explained as follows: as the setback layer is thicker, the remote impurity scattering from the supply layer becomes weaker, so in the beginning the mobility increases. When the thickness of the setback layer is further increased, the electron screening becomes weaker due to lower electron density in the Si QW layer. Thus, mobility drops even though the remote scattering is reduced with a longer setback distance.

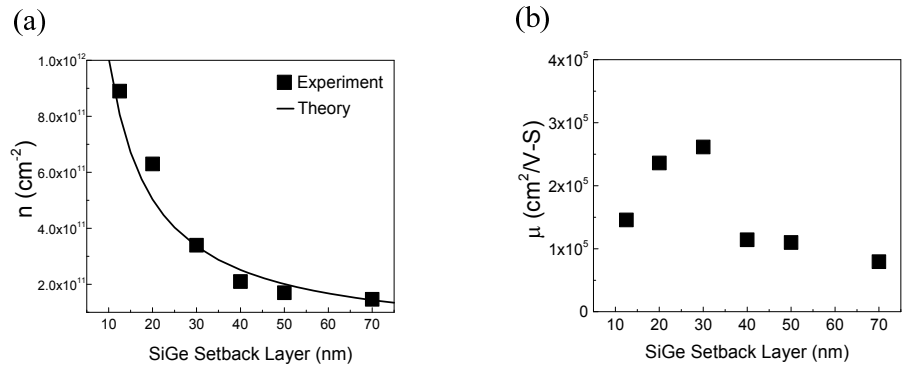

Fig. A.13 (a) Electron density and (b) mobility vs. SiGe setback layer thickness at 4 K.

B. Isotopically Enriched ^{28}Si 2DEGs

B.1 Introduction

In 2005, Petta *et al*. demonstrated the first spin-based quantum computing in a double quantum dot device on a GaAs two-dimensional electron gas (2DEG) [B1]. However, the strong decoherence exists in a GaAs-based QD due to the hyperfine interactions of electron spins and nuclear spins. On the other hand, for Si QDs, much reduced spin decoherence was demonstrated with a longer dephasing time (T_2^*) [B2] due to the lower fraction of the only nuclear-spin-carrying isotope of ^{29}Si (4.7 %) [B3]. Moreover, ^{29}Si can be reduced by ^{28}Si enrichment [B4] and less spin decoherence is predicted [B5]. Thus, in the first part of this section, we present the work on the electron transport properties of enriched ^{28}Si 2DEGs.

B.2 Isotopically Enriched ^{28}Si 2DEGs

Quantum dots (QDs) containing single electrons are very promising for the realization of spin-based quantum computing in solid-state systems due to their scalability and the mature semiconductor technology. A coherent control over the spin states of two single electrons in a double quantum dot was demonstrated in GaAs for the first time [B1]. However, its short dephasing time T_2^* ~ 7 ns of electron spins due to the severe hyperfine interactions with the host nuclei [B6] imposes a restriction on the speed of gate switching to preserve the quantum phase information before a gate switching operation is completed. To increase the dephasing time of electron spins, silicon has been suggested a replacement because of the very little spin decoherence resulting from its only spin-carrying isotope ^{29}Si of 4.7 % [B3]. A much longer T_2^* ~ 360 ns was recently demonstrated in a Si double QDs [B2]. With the reduction of ^{29}Si to below 0.01 %, a very long dephasing time has been predicted due to the much suppressed hyperfine interactions between electron spins and nuclear spins of ^{29}Si [B5].

While a 2DEG in an isotopically-enriched ^{28}Si quantum well (QW) was demonstrated by molecular beam epitaxy (MBE) with the mobility of 55,000 cm^2/V-s at density of 3×10^{11} cm^{-2} [B4], the reason of its relatively low electron mobility compared to Si 2DEGs of natural abundance and the limiting factor of electron scattering are still unknown. Moreover, there is no report yet on an enriched ^{28}Si 2DEG prepared by CVD. Thus, we study the transport properties of enriched ^{28}Si 2DEGs by CVD and estimate the spin decoherence in this section.

The preparation of enriched ^{28}Si 2DEG samples was similar to the steps described in section A except that a specialized silane of enriched ^{28}Si was used a gas precursor. After cleaning steps, relaxed SiGe

substrates were loaded into the CVD reactor for epitaxial growth. A SiGe buffer layer of 100 ~ 150 nm was first grown at 575 ^{o}C, followed by a strained-Si layer (2DEG layer) at 625 ^{o}C , a SiGe setback layer at 575 ^{o}C, a n-type SiGe supply layer at 575 ^{o}C, a SiGe cap layer at 525 ^{o}C, and a Si cap layer at 625 ^{o}C (Table B.1). There are two sets of samples in this section. First, a depletion-mode device of modulation-doped 2DEG with ^{28}Si enriched throughout the entire epitaxial growth (including Si and SiGe epitaxial layers) was fabricated. For enhancement-mode samples, the supply layer was grown without n-type doping and ^{28}Si was only enriched in the Si QW layer.

Table B.1 Layer structures of isotopically enriched ^{28}Si 2DEGs

Layer (nm)	Modulation-Doped	Undoped
Si cap	7	3
SiGe cap	25	0
SiGe supply	10	0
SiGe setback	25	
Si quantum well	16	9*
SiGe buffer	110	150

* ^{28}Si was only enriched in the Si quantum well.

B.2.1 Reduction of Spin-Carrying Isotope ^{29}Si by ^{28}Si Enrichment

The concentrations of three isotopes ^{28}Si, ^{29}Si, and ^{30}Si, and Ge vs. depth in a modulation-doped enriched ^{28}Si 2DEG device are shown in Fig. B.1. Below the growth interface at 185 nm, the fractions of ^{28}Si, ^{29}Si, and ^{30}Si are 92, 4.7, and 3.3 %, respectively, which are identical with the compositions of the natural isotopic abundance [B3]. For Si and SiGe epitaxial layers grown with silane of enriched ^{28}Si, the fractions for those three isotopes became 99.72, 0.08, and 0.002 %, respectively. The enrichment factors defined as the ratios of ^{28}Si to ^{29}Si and ^{28}Si to ^{30}Si were increased from 20 to 1250 (60 times enhancement), and 27 to 50,000 (2000 times enhancement), respectively.

We now estimate the potential impact of ^{28}Si enrichment on the spin decoherence in Si QDs. By the enrichment of ^{28}Si, the spin decoherence of QD electrons from the nuclear spins of ^{29}Si can be much suppressed. This would reduce the dephasing time (T_2^*), which is dominated by the hyperfine interactions between nuclear spins and electron spins. Assuming 10^5 nuclei in a Si QD of 100 nm $\times$ 100 nm, Assali *et al.* proposed a numerical model to estimate the dephasing time in Si

$$T_2^* = \frac{\hbar}{4.3e\sqrt{10^5 r}} \times 10^{11} \quad \text{(B.1)}$$

where *e* is electron charge and *r* is the fraction of ^{29}Si. The predicted dephasing time versus *r* was shown in Fig. B.2 and compared with experimental results of a GaAs QD and a Si QD of natural abundance. Maune *et al*. reported the first dephasing time of 360 ns in a Si double QDs of natural abundance [B2], which is 50 times longer than that in a GaAs QD and very close to Assali's prediction. In our sample, the fraction of ^{29}Si was purified by a factor of 20 to 0.08% and the dephasing time is expected to be 2 μs, two orders of magnitude longer than that of a GaAs QD and 6 times longer than that of a Si QD of natural abundance. According to the model, if ^{29}Si can be reduced to 10 ppm, the decoherence can be much avoided with T_2^* longer than 10 μs.

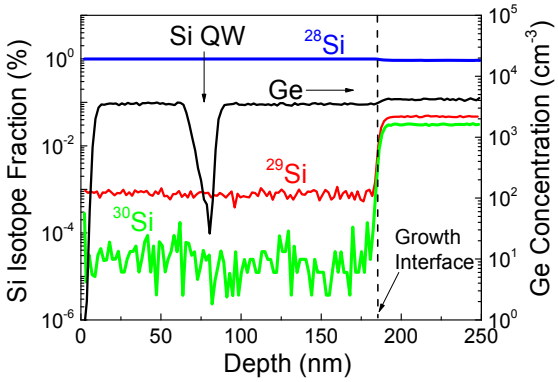

Fig. B.1 Three isotopes ^{28}Si, ^{29}Si, and ^{30}Si vs. depth in 2DEG structure with Ge as an indicator by SIMS measurements. The growth started at the depth of 185 nm and Si QW is at the depth 75 nm.

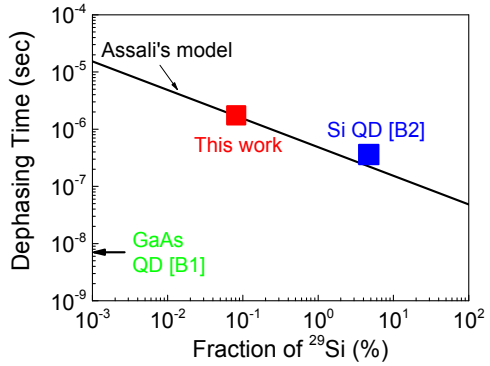

Fig. B.2 Dephasing time vs. ^{29}Si fraction. Solid line is the model prediction, the blue square is the experimental result in Si QD [B2], and the red square represents the predicted time in our samples. Dephasing time of GaAs QDs [B1] is also presented for comparison.

B.2.2 Magneto-transport Properties of Modulation-Doped Enriched ^{28}Si 2DEG

For the depletion-mode device, Hall electron density at 4 K was 4 × 10^{11} cm^{-2} with mobility of 399,000 cm^2/V-s. The longitudinal (R_{xx}) and transverse (Hall) resistances (R_{xy}) were also measured at 0.3 K with the magnetic field up to 8 T (Fig. B.3). The onset of Shubnikov-de Haas (SdH) oscillations in R_{xx} occurs at 0.4 T. The spin splitting due to the associated Zeeman energy difference exceeding the Landau level broadening occurs at 0.75 T with filling factor of ν = 24. The revelation of the two-fold degeneracy from two valleys of density of states was observed at 1.9 T with ν = 9. For Hall resistance (R_{xy}), the quantum Hall structures can be resolved at B = 0.7 T with the filling factor of ν = 24 and clear plateaus were observed at ν = 2, 4, 8 etc. The two-dimensional electron densities extracted from SdH oscillations and low-field Hall resistance were 4.02 and 4.18 × 10^{11} cm^{-2}, respectively, showing that parallel conduction is insignificant. The electron mobility of this device at 0.3 K was 522,000 cm^2/V-s with an associated mean free path of 6 μm, which we believe is the highest reported for modulation-doped Si 2DEGs grown by CVD regardless of ^{28}Si enrichment. In previous work of isotopically enriched ^{28}Si, the highest reported mobility was 55,000 cm^2/V-s in a MBE-grown 2DEG. Our results established the extremely high quality in our isotopically enriched samples.

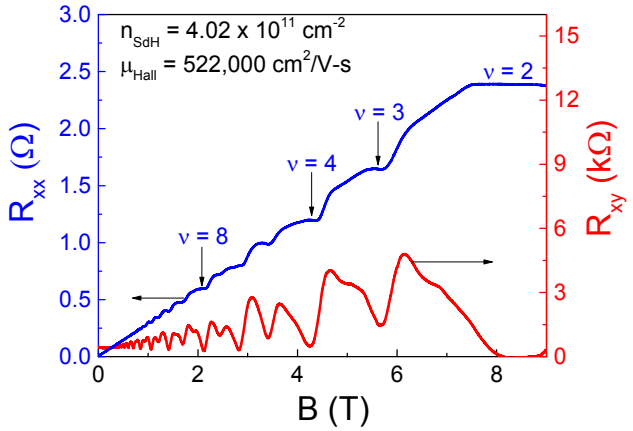

Fig. B.3 Magneto-resistances of depletion-mode enriched ^{28}Si 2DEG device measured at 0.3 K. Electron density (4. × 10^{11} cm^{-2}) and mobility (522,000 cm^2/V-s) were extracted from the periods of Shubnikov-de Haas oscillations in longitudinal resistance (R_{xx}) vs. (1/B) and its value at zero field.

B.2.3 Gating of Enhancement-Mode Enriched ^{28}Si 2DEGs

For quantum dot devices, a short distance between the surface and 2DEG layer is preferred for fine gate control. Thus, we chose shallow 2DEGs of SiGe setback layer < 150 nm. Three enhancement-mode devices of undoped enriched ^{28}Si only in Si QW layer were made without n-type dopants with a SiGe setback layer of 60 and 150 nm (Table B.1). There is no parallel conduction from n-type supply layer in these undoped enhancement-mode devices. Besides, since the Si surface layer was thin (< 3 nm), the quantum states in that layer are higher than the Fermi level, eliminating the potential parallel conduction at the surface. Furthermore, considering the intimate proximity with Si/Al_2O_3 interface, the surface conduction is negligible because of the strong scattering from the interface impurity and roughness compared to the conduction in the 2DEG layer. Thus, the measured Hall density and mobility are considered the representation of 2DEG transport properties in this work.

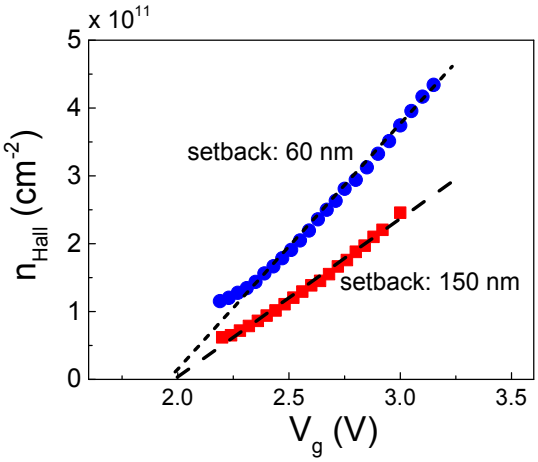

Fig. B.4 Electron density vs. gate voltage by Hall measurement at 4 K for enhancement-mode devices of enriched ^{28}Si 2DEG with a SiGe setback layer of 60 and 150 nm. The slopes represent the effective capacitance between a Cr/Au gate and 2DEG.

With a metal gate of Cr/Au on top of 90-nm Al_2O_3, the electron density and mobility in 2DEG layer can be modulated and the dominant scattering mechanisms could also be justified by checking μ vs. n

relation with different thicknesses of SiGe setback layer (60 and 150 nm). The electron density vs. gate voltage of those two samples was shown in Fig. B.4. The capacitance extracted from the slopes are 5.8 $\times$ 10^{-8} F/cm^2 and 4.1 $\times$ 10^{-8} F/cm^2 for the setback layer of 60 and 150 nm, respectively, within 5 % of the calculated values based on a parallel-plate capacitor model. The lowest density are 1.1 and 0.6 $\times$ 10^{11} cm^{-2} at V_g = 2.2 V, which we believed is the lowest density among all reported enriched ^{28}Si 2DEG. The extrapolation of n_{2D} vs. V_g to zero density gives the threshold voltage (V_T) around 2 V. Below V_g = 2.2 V. there was no conduction in the 2DEG channel because of the metal-insultaor transition (MIT) [B7]. By assuming the threshold voltage dominated by impurity charge (Q_{int}) at Si/Al_2O_3 interface, a simple estimation can be made with $Q_{int} = C_{ALO}V_T$ on the order of 10^{12} cm^{-2}.

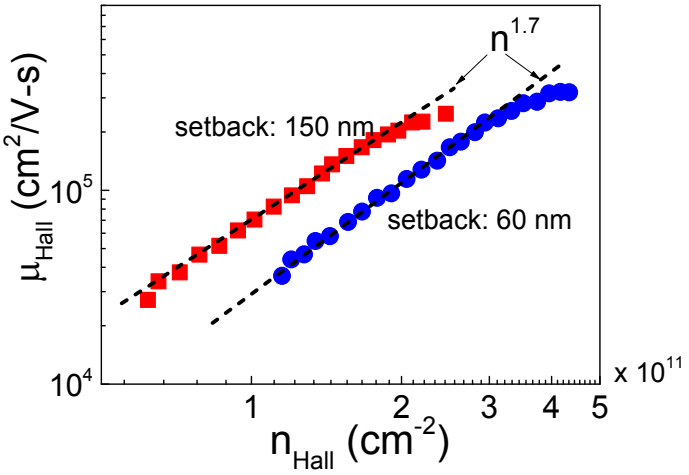

Fig. B.5 Hall mobility vs. density for enhancement-mode devices of enriched ^{28}Si 2DEG with a SiGe setback layer of 60 and 150 nm at 4 K.

In Fig. B.5, electron mobility vs. density at 4 K for these enhancement-mode devices is illustrated. For device of 150-nm SiGe setback layer, the lowest density is 6.2 $\times$ 10^{10} cm^{-2} with mobility of 28,000 cm^2/V-s. Below this critical density, electron conduction ceased because MIT occurs. For both devices, the mobility scales with the density as $\mu \propto n^{1.7}$. Based on the previous work [A20, B8], if the 2DEG is limited by the remote impurity scattering, then α = 1.5. Thus, we concluded that the major source of electron scattering in these enriched ^{28}Si 2DEG devices is the remote impurity at the Si/Al_2O_3 interface.

C. Solving Phosphorus Segregation in SiGe for Effective Schottky Gating

C.1 Introduction

As the device dimensions are scaled down, a sharp profile of dopants is becoming a key factor to realize nano-scale semiconductor devices such as two-dimensional electron gases (2DEGs) in a modulation-doped Si/SiGe heterostructure [C1]. 2DEGs are of particular interest for quantum dot (QD) applications. A QD is usually fabricated on a 2DEG, with top metal Schottky depletion gates used to isolate a single electron in the underlying 2DEG layer. However, the strong surface segregation of n-type dopants in a relaxed SiGe epitaxial film can cause a high dopant concentration at the surface, resulting in high gate leakage current and ineffective gating. Therefore, a sharp turn-off slope of n-type dopants is necessary.

Although a turn-off slope of 2-3 nm/dec for antimony was reported in Si epitaxial films grown by molecular beam epitaxy (MBE) [C2], it has been difficult to obtain such abrupt profiles for phosphorus and arsenic, the most common n-type dopants in chemical vapor deposition (CVD) systems [C3]. Several works were reported to reduce phosphorus segregation in Si by ex-situ cleaning (13 nm/dec) [C4] or by introducing substitutional carbon atoms into Si epitaxial films (11 nm/dec) [C5]. However, the former approach requires a growth interruption, which may introduce contaminants into the growth interface. For the latter, the control over carbon atoms into substitutional sites is critical since the interstitial carbon could degrade device performance due to their midgap energy states [C6].

We report an extremely sharp phosphorus turn-off slope of 6 nm/dec in relaxed $Si_{0.7}Ge_{0.3}$ films without any ex-situ cleaning step or introduction of carbon into the epitaxial films. We found that the hydrogen coverage on the surface during the growth plays an important role in the suppression of phosphorus segregation in the CVD process at low temperatures (500 ~ 600 ^{o}C). Finally, a phenomenological model is proposed to explain the effect of surface hydrogen on phosphorus segregation.

C.2 Modeling phosphorus segregation: Two State Model

In our work, a matrix of Si and Ge atoms and surface hydrogen complicate the analysis of phosphorus segregation. In a simpler case of P in Si (100), a segregation energy of 0.64 eV was firstly reported by Nützel *et al*. [C7] from SIMS results. This work used a so-called two-state model (TSM) [C8] of P atoms moving between the surface and sub-surface layers in Si. Later, by temperature programmed desorption (TPD), Cho *et al*. [C9] reported a segregation enthalpy of 0.86 eV, which is defined as free energy of phosphorus in surface and bulk layers, essentially the same as the segregation energy defined in the TSM. The P coverage in their study was larger than 0.1 monolayer (ML) and the major Si surface structures with P surface coverage > 0.1 ML was previously proposed by Yu *et al*. [C10] as a mixture of Si–Si, Si–P, and P–P dimers. Sen *et al*. [C11] used density functional theory to predict the different favorable sites for surface P atoms at coverage above and below 0.13 ML. Thus, the work in [C10, C11] might not be directly relevant to our experimental results since the integrated P doses in our samples are at most 5×10^{12} cm^{-2} (~ 0.01 ML). Other works on Sb [C12], As [C13], and Ge [C14, C15] surface segregation in Si have also been modeled by using a TSM. In addition, those works all ignored any temperature dependence of attempt frequency and used the segregation energy to reflect all temperature effects. Thus, in this section, we also use a modified TSM to investigate phosphorus segregation in a more complicated structure of relaxed $Si_{0.7}Ge_{0.3}$ layers.

A two-state model (TSM) describes the dopant segregation as an exchange process of P atoms and host atoms (Si or Ge in this study) between the surface layer and the sub-surface layer (Fig. C.1). The rate equations governing this exchange process between those two layers are

$$\frac{dn_1}{dt} = -r_{12}n_1(1-n_2) + r_{21}n_2(1-n_1), \tag{C.1}$$

$$\frac{dn_2}{dt} = -r_{21}n_2(1-n_1) + r_{12}n_1(1-n_2), \tag{C.2}$$

$$r_{12} = \nu e^{-\frac{E_1}{kT}}, \tag{C.3}$$

$$r_{21} = \nu e^{-\left(\frac{E_1+\Delta E_{surf}}{kT}\right)}, \tag{C.4}$$

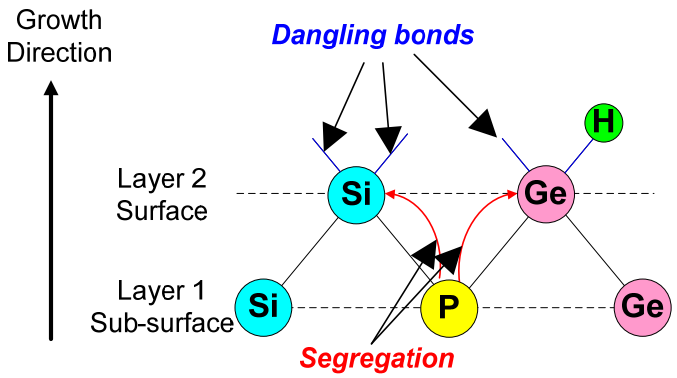

Fig. C.1 Schematic of atomic layer structures near the surface during the epitaxial growth.

where n_1 and n_2 are the normalized concentrations of phosphorus in the sub-surface layer (layer 1) and the surface layer (layer 2), r_{12} and r_{21} are the jumping rates of phosphorus from the sub-surface layer to the surface layer, and vice versa. E_1 is the activation energy barrier facing phosphorus in the sub-surface layer, ΔE_{surf} is the segregation energy, which represents the difference of activation barriers of layer 1 and layer 2, and v is the attempt frequency (Fig. C.2). We assume a single attempt frequency independent of temperature as previous reports suggested for phosphorus segregation in Si [C7, C8, C9, C13, C14, C15]. It is assumed that P atoms below the sub-surface layer are trapped and cannot diffuse during the time scale of the growth. Assuming n_1 and n_2 << 1, the differential rate equations can be solved and an analytical form of phosphorus turn-off slope x_0 (nm/decade) is given [C16]

$$x_0 = \frac{a_0 \ln 10}{4} \frac{1}{\ln\left(1+e^{\frac{-\Delta E_{surf}}{kT}}\right) - \ln\left[1-e^{-[r_{12}+r_{21}]\frac{a_0}{4GR}}\right]}, \qquad \text{(C.5)}$$

where a_0 is lattice constant and GR is the growth rate.

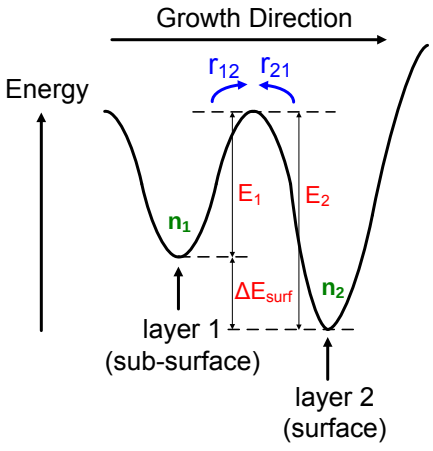

Fig. C.2 Schematic of phosphorus energy near the surface during the epitaxial growth in a two-state model. Layer 2 represents the surface layer and layer 1 (sub-surface layer) represents the next layer below the surface.

According to the TSM, the surface segregation occurs because P atoms at the sub-surface layer tend to jump to the surface layer due to the lower energy level in the surface layer (Fig. C.2). At thermal

equilibrium (low growth rates), the surface segregation is determined by the ratio of the phosphorus concentrations at the surface and sub-surface layers (n_2/n_1), which only relies on the temperature and the segregation energy (ΔE_{surf}) through the first term in the denominator of Eq. (C.5). At lower temperatures, if still in equilibrium, more P atoms are trapped in the surface layer than in the sub-surface layer due to the lower energy state of the former, so the segregation is stronger. On the other hand, in the kinetic-limited regime of high growth rates, P atoms in the sub-surface layer cannot reach the equilibrium with those in the surface layer. Therefore, phosphorus will be trapped in the sub-surface layer and the limiting factor is its activation energy barrier E_1. As the temperature is reduced, the probability of phosphorus jumping across the barrier to the surface layer is smaller because of the less kinetic energy of phosphorus. As a result, phosphorus segregation is reduced. This physical limit has been applied to reduce phosphorus segregation in Si (100) grown by MBE at temperature below 500 ^{o}C [C7] and the best turn-off slope (4 nm/dec) for P in Si was reported by room-temperature growth [C17].

C.3 Failure of Two-State Model and discrepancy resolution

C.3.1 Experimental Results

Si (100) substrates (for strained SiGe) and polished relaxed $Si_{0.7}Ge_{0.3}$ virtual substrates with a graded $Si_{1-x}Ge_x$ ($0 < x < 0.3$) buffer layer grown on Si (100) substrates (for relaxed SiGe) were used to study phosphorus segregation. Prior to being placed into the reactor, substrates were cleaned by the following steps: 5 min in diluted HF (1%), 15 min in H_2SO_4: H_2O_2 (2.5:1), followed by 2 min in diluted HF (1%). Then the samples were heated to 850 ^{o}C in a hydrogen carrier at 6 torr to remove the residual oxide before the epitaxial growth starts. The gas precursors were diluted silane (10 % in argon) and GeH_4 (0.8 % in hydrogen) for Si and SiGe growth, and a diluted phosphine was the doping gas. The test structure for phosphorus segregation is as follows: first, a 20-nm undoped $Si_{0.7}Ge_{0.3}$ buffer layer was grown followed by a 10-nm n-type $Si_{0.7}Ge_{0.3}$ layer doped with phosphorus of peak level between 10^{18} to 10^{19} cm^{-3}. Both layers were grown at 575 ^{o}C and the growth rate was 5 nm/min. Then an undoped $Si_{0.7}Ge_{0.3}$ cap layer was grown at 500 ^{o}C ~ 600 ^{o}C to study the effect of growth temperature on phosphorus segregation with its thickness between 30 to 150 nm. To investigate the effect of growth rate, we varied the growth rate of the $Si_{0.7}Ge_{0.3}$ cap layers between 0.1 to 30 nm/min by adjusting the partial pressures of silane and germane. The Ge fraction in the SiGe cap layer was between 0.28 to 0.30. Last, a thin Si cap layer of 4 nm was grown at 625 ^{o}C with the growth rate of 2.5 nm/min. The films were subsequently characterized by SIMS to determine the phosphorus profiles and the growth rates.

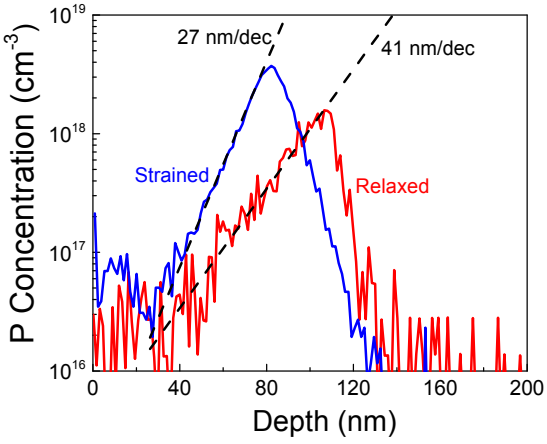

Fig. C.3 Phosphorus profiles in strained and relaxed $Si_{0.7}Ge_{0.3}$ layers grown at 575 ^{o}C [C16].

Most prior works of phosphorus segregation in SiGe were done in compressively strained SiGe layers [C13], not in the relaxed SiGe layers required for a modulation-doped 2DEG, i.e. a higher conduction band in a SiGe layer than in a Si layer. Thus, we compared the phosphorus profiles in strained and relaxed SiGe films first. We found that the segregation is much worse in relaxed SiGe films than in strained SiGe films (Fig. C.3). For a growth temperature of 575 °C and growth rate of 5 nm/min, the turn-off slopes of phosphorus in strained and relaxed films are 27 and 41 nm/decade, respectively [C16]. The fundamental reasons for this difference are unknown and a further study is required. We then focused on phosphorus segregation in the relaxed $Si_{0.7}Ge_{0.3}$ films.

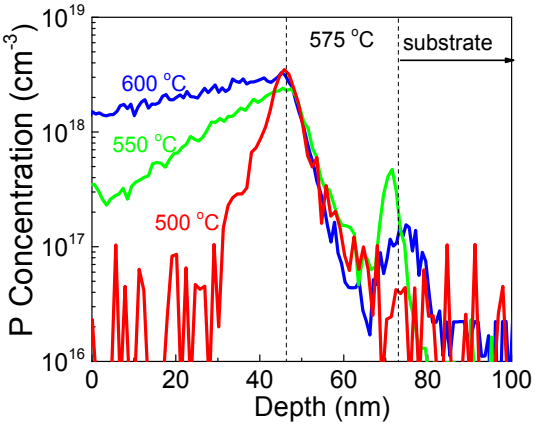

Fig. C.4 Phosphorus profiles in relaxed $Si_{0.7}Ge_{0.3}$ layers grown at 500, 550, and 600 °C. Phosphorus supply was turned off at the depth of 45 nm. P turn-off slopes were 127, 40, and 9 nm/decade for 600, 550, and 500 °C, respectively [C16].

Phosphorus profiles measured by SIMS for relaxed SiGe layers grown at 500, 550, and 600 °C are shown in Fig. C.4. At a depth of 45 nm, the phosphine supply for the doped layer was turned off. As the growth temperature is reduced, the surface segregation is reduced with the phosphorus turn-off slope declining from 127 nm/dec at 600 °C to 9 nm/dec at 500 °C. By adjusting the gas flow rates of silane and germane at 500 °C, an extremely sharp profile of 6 nm/dec was obtained with the growth rate of 0.08 nm/min, which we believe is the sharpest reported turn-off slope of phosphorus in relaxed SiGe films.

Our experimental data (points) of phosphorus turn-off slope vs. growth rate at different temperatures (500 °C to 600 °C) and theoretical curves based on the TSM are shown in Fig. C.5. At 600 °C the segregation is near the transition between thermal equilibrium and kinetic-limited regime. Thus, ΔE_{surf} = 0.47 eV can be fitted by assuming the experimental results were in the regime of thermal equilibrium. Furthermore, as Nützel *et al*. [C18] suggested that the attempt frequency would be between 10^{11} to 10^{13} Hz, we selected $\nu = 1 \times 10^{12}$ Hz to fit the data at 600 °C and found E_1 = 1.84 eV. Despite a good match between the experimental data and the theoretical curve at 600 °C, there is a large discrepancy between them (500 °C ~ 575 °C). The low dependence of the segregation on growth rate suggests the data at low temperatures were in the equilibrium regime, not kinetically limited. However, the phosphorus slopes are much sharper at lower temperatures, in contrast with what would be expected from the TSM in equilibrium. This discrepancy cannot be resolved by simply adjusting the fitting parameters.

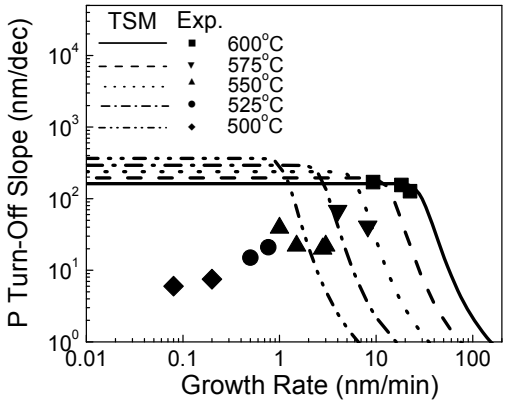

Fig. C.5 Phosphorus turn-off slope vs. growth rate for different temperatures. Experimental results (points) and the theoretical prediction (lines) are presented for comparison [C16].

C.3.2 Effects of Hydrogen on Phosphorus Segregation

In the CVD process, hydrogen is used as a carrier gas and it is well established that hydrogen could cover the surface by forming Si–H or Ge–H bonds [C19]. At high temperatures, most of those bonds break easily and hydrogen desorbs, so the surface coverage of hydrogen is nearly zero. At low temperatures, however, the thermal energy is too low to break the Si–H or Ge–H bonds efficiently, so hydrogen will cover most of the surface layer. Our data show that the phosphorus turn-off slope is nearly constant with growth rate at a fixed temperature, suggesting that it is in the regime of thermal equilibrium, with segregation depending on ΔE_{surf}. At the heart of our model, we assume phenomenologically that the presence of surface hydrogen changes the relative energy of P atoms in the surface and sub-surface layers such that the segregation energy ΔE_{surf} is reduced. Thus, at lower temperatures, segregation will be suppressed due to higher hydrogen coverage on the surface. Because of two types of surface sites (with or without H), in principle we could model the problem with two segregation energies and a fraction of phosphorus segregation to each site. However, the two energies could probably depend on the local numbers of Si or Ge atoms, leading to too many parameters. Prior works by MBE and TPD used an effective segregation energy [54, 55] to investigated the effect of hydrogen on Ge segregation into Si (100), which we follow in this study. Thus, we treat ΔE_{surf} as a single effective parameter which varies with hydrogen coverage as temperature changes.

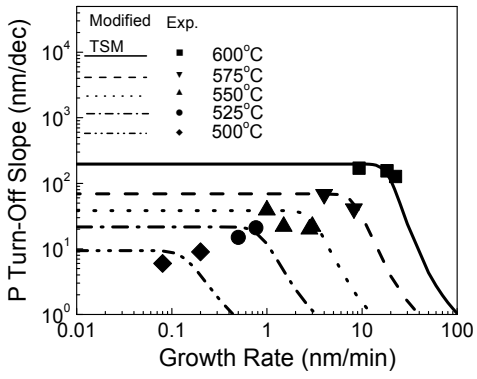

Fig. C.6 Comparison of experimental data and modified TSM of phosphorus turn-off slope vs. growth rate by including the effect of surface hydrogen on the segregation energy (E_{surf}) [C16].

By introduction of hydrogen effect on phosphorus segregation, a fit between the experimental data and the model is obtained by using ΔE_{surf} as a fitting parameter (Fig. C.6) with ΔE_{surf} plotted vs. temperature in Fig. C.7. At hydrogen pressure of 6 torr, the reduced segregation at lower temperatures originates from a smaller segregation energy ΔE_{surf}. The decrease of ΔE_{surf} with decreasing temperature will reduce the ratio of phosphorus populations in the surface vs sub-surface layers (n_2/n_1), resulting in a reduction of the segregation. On the other hand, ΔE_{surf} increases with temperature because of less H coverage at higher temperatures. The reduced segregation energy of P in $Si_{0.7}Ge_{0.3}$ with more H coverage surface follows the trend of Ge segregation in Si [C14, C15, C20]. To confirm that the main effect of segregation reduction comes from a change of H coverage rather than a change of attempt frequency or other effects with temperature, we adjusted hydrogen pressure to vary its surface coverage [C21] at 575 ^{o}C (Fig. C.7). As expected, with higher hydrogen pressure (23 torr), the segregation is suppressed, leading to a lower effective segregation energy and the opposite trend is shown with a lower hydrogen pressure of 2 torr. The segregation energy obtained in this work ranges between 0.37 ~ 0.52 eV, which is lower than those published for P in Si of 0.67 ~ 0.86 eV [C7, C9] without hydrogen coverage. The difference could be explained by the presence of surface hydrogen on $Si_{0.7}Ge_{0.3}$ surface in this work.

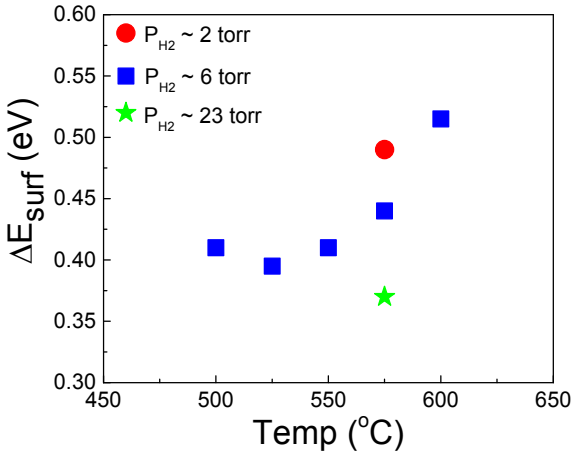

Fig. C.7 Segregation energy (E_{surf}) vs. growth temperature. At 575 ^{o}C, E_{surf} for hydrogen pressure of 2, 6, 23 torr are also plotted to confirm the effect of surface hydrogen on P surface segregation [C16].

D. Inverted Modulation-Doped Si 2DEG and Double Si 2DEG with Thin Barrier

D.1 Introduction

Inverted structures are crucial for the realization of bilayer devices with two adjacent 2DEGs with a thin tunneling barrier in between [D1]. While a GaAs-based bilayer device has been successfully fabricated by the delta-doping technique [D2], there is no experiment reported on Si bilayer devices yet. The major obstacle for the demonstration of a Si bilayer device is the severe surface segregation of n-type dopants, which would swamp the mobility in the bottom channel of Si 2DEG due to stronger impurity scattering from n-type dopants in the setback layer. While a sharp arsenic turn-off by ion implantation for the bottom n-type doping layer in an inverted Si 2DEG device was reported [D3], the mobility was limited by the defects induced during implant process and the quality of the re-growth interface. Furthermore, high temperature annealing is required to activate the dopants and remove the defects by implant, which would induce strain relaxation and increase the thermal budget for the subsequent processing steps. By low-temperature epitaxy the phosphorus segregation can be significantly reduced with a sharp

turn-off, enabling a low level in the setback layer. Thus, we investigate the effect of phosphorus segregation on 2DEG characteristics and present the highest reported mobility of 470,000 cm^2/V-s for all inverted modulation-doped Si 2DEGs.

D.2 Effects of Phosphorus Turn-off Slope

To investigate the effects of phosphorus segregation on 2DEG properties in an inverted structure, three samples of different phosphorus turn-off slopes (40, 14, and 8 nm/decade) were grown at different temperatures. The details of the layer structures are listed in Table D.1 and the associated SIMS results are illustrated in Fig. D.1. For those three samples, the thickness of the setback layer is defined as the distance between phosphorus peak and the lower Si/SiGe heterojunction. Hall electron density and mobility measured at 4 K are plotted versus phosphorus turn-off slope in Fig. D.2.

Table D.1 Layer structures of sample #5457, #5850, and #5630 to study the effects of P turn-off slope on 2DEG characteristics in an inverted modulation-doped structure.

Sample #	5457	5850	5630
Si cap (nm)	5	3	2.5
SiGe cap (nm)	46	38	50
Si QW (nm)	12	11	11
SiGe setback (nm)	20	20	33
P Peak level (cm^{-3})	4.8×10^{18}	3.3×10^{18}	4.6×10^{18}
SiGe buffer (nm)	160	125	170

The Hall electron densities of sample #5457, #5850, and #5630 are 3.8×10^{12} cm^{-2}, 7×10^{11} cm^{-2}, 1.8×10^{11} cm^{-2}, respectively. Since the setback layer of #5630 is thicker, for a comparison of electron density in a fixed setback distance, a simple correction step based on Poisson's equation (Eq. (A.2)) was performed. The corrected density is 2.7×10^{11} cm^{-2} (open triangle in Fig. D.2) and a clear trend of increasing density with phosphorus turn-off slope is observed. As P turn-off slope increases, there is more phosphorus in the SiGe setback layer, which would effectively reduce the setback distance by transferring electrons in shorter distances, leading to higher density.

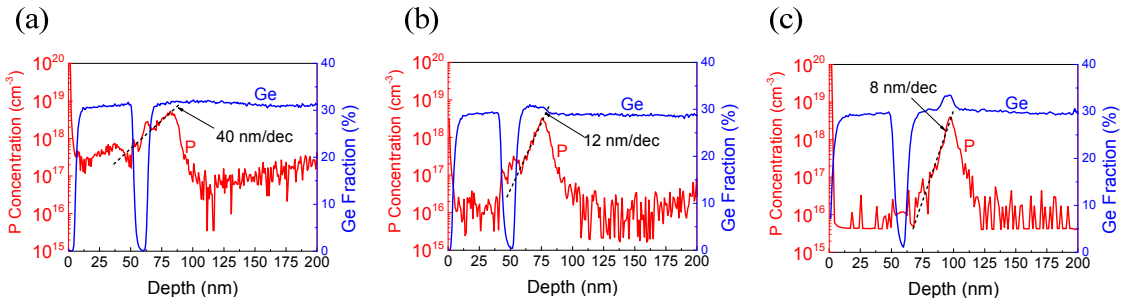

Fig. D.1 P and Ge profiles of sample #5457, #5850, and #5630. P turn-off slopes of these three samples are 40, 14, and 8 nm/dec, respectively. The setback layer thicknesses between the phosphorus peak level and the lower Si/SiGe heterojunction are 20, 20, and 33 nm for those three samples.

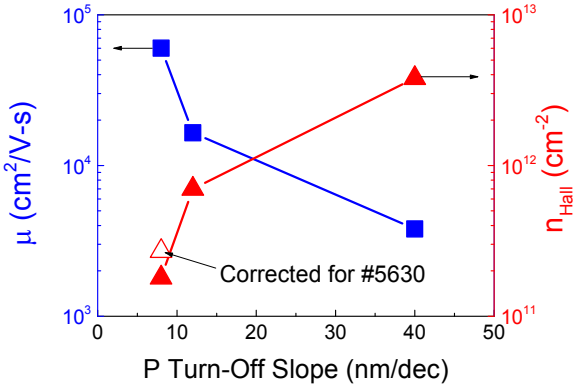

Fig. D.2 Hall density and mobility vs. P turn-off slope for sample #5457 (40 nm/dec), #5850 (14 nm/dec), and #5630 (8 nm/dec). A corrected electron density was calculated by Poisson's equation to compensate the effect of the thicker SiGe setback layer in sample # 5630.

2DEG mobility is also greatly affected by phosphorus turn-off slope (Fig. D.2). With a fast phosphorus turn-off slope of 8 nm/dec in sample #5630, the mobility is 60,000 $cm^2/V\text{-}s$, 20 times higher than that of sample #5457 with a slow slope of 40 nm/dec. For sample #5457, even though the electron screening is expectedly stronger than that of sample #5630 due to the higher electron density (3.8×10^{12} cm^{-2} >> 1.8×10^{11} cm^{-2}), the mobility is actually much lower. This is attributed to the high level of phosphorus in the setback layer because of a slow phosphorus turn-off, introducing stronger scattering for 2DEG.

D.2.1 Effects of Remote Impurity at the Si/Al_2O_3 Interface

Here, we study the effect of the impurity charges at the Si/Al_2O_3 interface. Unlike a top modulation-doped Si 2DEG with ionized impurities in the supply layer screens remote charges at Si surface, in an inverted structure, the remote scattering effect of surface charges must be considered because of the absence of n-type doping layer between the surface and 2DEG. If the charge density at the surface is higher than the remote impurity charge in the bottom supply layer in an inverted 2DEG device mobility will be affected [D4]. By reducing the surface charge density or the distance between the surface and 2DEG, the scattering is expected to be weaker [A11].

Hall bar devices with a $Cr/Al/Al_2O_3$ gate stack on top of inverted modulation-doped Si 2DEGs were fabricated to investigate the effect of the surface charges on 2DEG transport. Two samples of different thicknesses of top SiGe cap layer, which separates the surface charge and 2DEG were grown (Table D.2). SIMS profiles of these two samples are plotted in Fig. D.3. The levels of phosphorus background are as low as SIMS detection limit, of 4×10^{15} cm^{-3}, so the background impurity scattering is not considered the dominant scattering mechanism.

Table D.2 Layer structures of sample #5877 and #5630 to study the effects of impurity charges at the Si/Al_2O_3 interface on 2DEG mobility.

Sample #	5877	5630
Si cap (nm)	3	2.5
SiGe cap (nm)	26	50
Si QW (nm)	11	11
SiGe setback (nm)	62	33
P Peak level (cm^{-3})	2.5×10^{18}	4.6×10^{18}
SiGe buffer (nm)	115	170

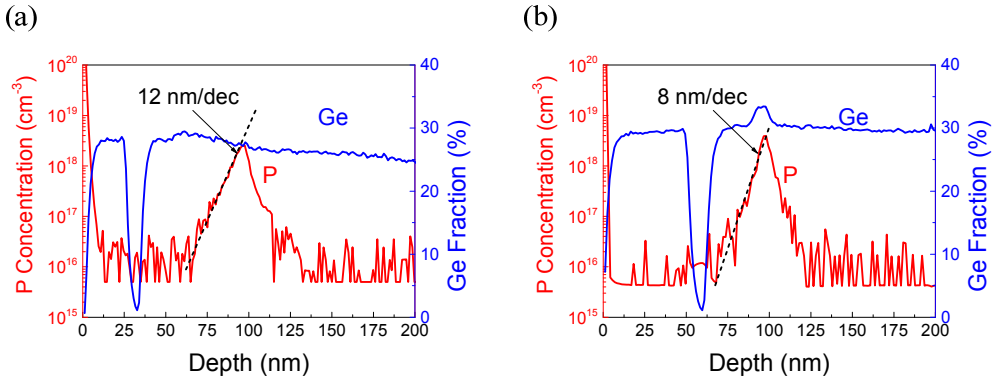

Fig. D.3 SIMS profiles of (a) #5877 and (b) #5630 of different top SiGe cap thicknesses.

Mobility vs. density for these two devices is plotted in Fig. D.4. The mobility of #5877 (26-nm SiGe cap) is much lower than that of #5630 (50-nm SiGe cap), which is attributed to the stronger scattering from the remote scattering of surface charges with a shorter distance. Furthermore, the bottom SiGe setback layer of #5877 is 2 times larger than that of #5630, the remote impurity scattering at the bottom supply layer is weaker than that in #5630. Thus, we believe scattering is dominated by the remote impurities at Si/Al_2O_3 interface. In addition, the critical density for metal-insulator transition (MIT) in #5877 is higher, which also implies stronger remote scattering from the Si/Al_2O_3 interface.

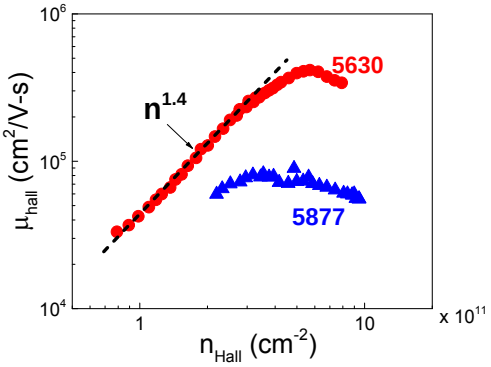

Fig. D.4 Hall mobility vs. density at 4 K for sample #5630 and #5877 for a comparison of the effect of upper Si cap layer thickness.

For #5630, an extremely low density, as low as 7.5×10^{10} cm^{-2} with mobility of 33,000 $cm^2/V\text{-}s$, was demonstrated. Very high mobility of 420,000 $cm^2/V\text{-}s$ at 4 K was achieved at density of 5.6×10^{11} cm^{-2}. The levels of the lowest density and the highest mobility in this inverted modulation-doped 2DEG device are comparable to those of the top doped 2DEGs, an indication of the effectiveness of low-temperature epitaxy, which enables low level of phosphorus in the setback layer and then greatly reduces the impurity scattering.

D.2.2 Second Subband Occupancy

For an enhancement-mode Si 2DEG device, interface roughness scattering was suggested by Huang *et al*. to account for the presence of peak mobility [A11]. Yet other mechanisms such as filling of the second subband could be the limiting factors. We present the analysis on sample #5630 and report the first observation of second subband occupancy in a Si 2DEG supported by our experimental results.

To explore the occupancy of second subband in Si QW layer, low-temperature measurement at 0.3 K was performed and Hall mobility vs. density is shown in Fig. D.6. There exist a peak mobility of 470,000 cm^2/V-s at density of 6.5 × 10^{11} cm^{-2} which is the highest reported for all inverted modulation-doped Si 2DEGs. Beyond this density, Hall mobility first drops to 330,000 cm^2/V-s at density of 7.7 × 10^{11} cm^{-2} and then rises again due to the presence of the second subband. This observation was explained by [101, 102, 103] as follows: (i) before the onset of the second subband occupancy, mobility increases due to the stronger electron screening with the electron density. (ii) As V_g increases, E_F enters the range of localized states of the second subband and some electrons scatter from the first band into those trap states, where electrons are immobile. Therefore, the effective Hall mobility of the electrons in the first band drops. (iii) Subsequently, as E_F is lifted up further by gating, those localized states are filled and electrons now populate at the second band and conduct by metallic screening. As a result, mobility starts to increase again with electron density. Note at density below 2.5 × 10^{11} cm^{-2}, mobility drops more sharply, which has been attributed to the occurrence of MIT.

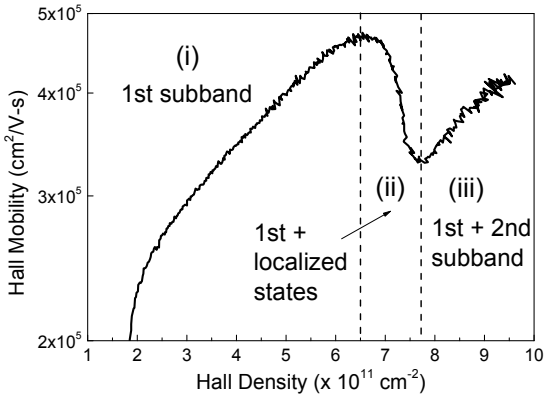

Fig. D.6 Hall mobility vs. density at 0.3 K for sample #5630. The onset of second subband occupancy occurs at density of 6.5 × 10^{11} cm^{-2}. In region (i), only the first subband is populated. For region (ii), some electrons in the first subband scatter into the localized states, so the mobility drops. In region (iii), electrons reside in both first and second subbands, so that the measured Hall mobility increases with electron density due to stronger screening.

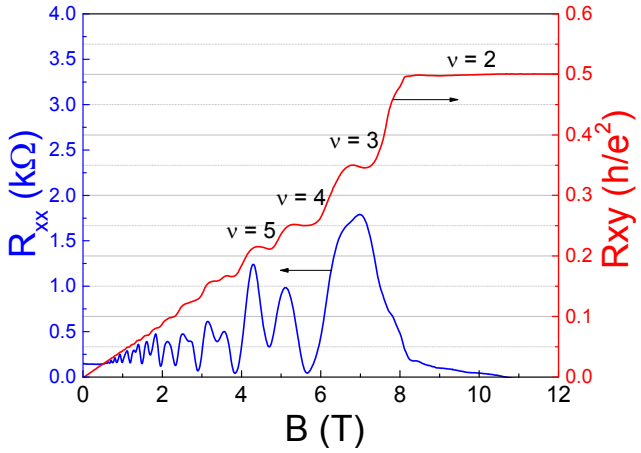

Fig. D.7 Magneto-resistances (R_{xx} and R_{xy}) vs. magnetic field at 0.3 K of sample #5630 at V_g = 3 V.

Magneto-resistances (R_{xx} and R_{xy}) vs. magnetic field at 0.3 K for sample #5630 at V_g = 3 V are shown in Fig. D.7. The onsets of Shubnikov-de Haas oscillations in R_{xx} and flat quantum Hall plateaus in R_{xy} occurred at 0.6 T and 0.9 T, respectively, showing the high quality of this inverted device. Spin and valley

splittings occurred at B = 1.3 T and 2.6 T respectively. It is interesting to note that there is no ν = 3 minima in R_{xx}, despite the presence of the Hall plateau in R_{xy}, which we do not understand yet. The vanishing longitudinal magneto-resistance (R_{xx}) indicates there is no parallel conduction from the bottom doping layer. Furthermore, a single period of R_{xx} vs. (1/B) suggests only one two-dimensional channel exists. As the gate voltage increases we observe beating in Shubnikov-de Hass oscillations indicating onset of the population of second subband.

A tentative sample of a bilayer device of two parallel 2DEGs was grown and SIMS results are shown in Fig. D.8. For the lower 2DEG, thickness of the setback layer is 35 nm with a peak level of phosphorus at 3.4 $\times$ 10^{18} cm^{-3}. The turn-off slope of phosphorus is ~ 20 nm/decade. Thickness of quantum wells is 10 nm, the wells are separated by a 3 nm SiGe barrier. For the upper 2DEG, the setback distance is 30 nm with phosphorus peak at 1 $\times$ 10^{19} cm^{-3} and a phosphorus turn-off slope of 22 nm/decade.

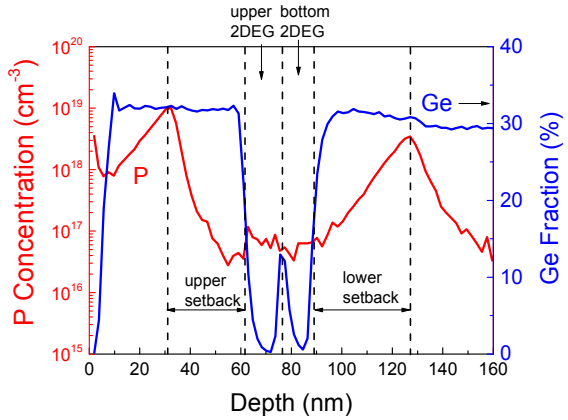

Fig. D.8 SIMS profiles of a bilayer device of two adjacent Si 2DEGs with a thin SiGe barrier of 3 nm.

E. Implant Isolation of Depletion-Mode Devices of Modulation-Doped Si 2DEG

E.1 Introduction

2DEGs are usually electrically isolated by mesa etching. However, the mesa edges can cause problems for subsequent fabrication steps, such as the application of electron-beam resist for sub-micron gates to form quantum dots and thin metal step coverage. In addition, in enhancement mode devices, high electrical fields in the gate insulator above the corner of the etched mesa may cause breakdown of the insulator or leakage currents.

Ion implantation for lateral electrical isolation ("implant isolation") on III-V materials has been a well-known technique for several decades [E6]. Ion bombardment creates deep defect levels, and these defects trap free electrons and pin Fermi level near mid-gap, resulting in high resistivity. This process not only provides excellent electrical isolation, but preserves the planarity of the surface. However, relatively few papers have focused on implant isolation in Si-based devices [E7], because the resulting high resistivity regions can't sustain post-isolation high-temperature process (>1000 ^{o}C) common in silicon technology. Furthermore, resistivity of the intrinsic silicon (Fermi level at mid-gap) is ~2 $\times$ 10^{5} Ω·cm at room temperature, which is not high enough for most applications. However, processing of Si/SiGe-based quantum devices is often constrained to be below 600 ^{o}C to avoid Si/Ge interdiffusion [E8], which could be low enough to avoid annealing of implant damage. Besides, the typical low operation temperature (4K or less) of quantum devices provides much less thermal energy for electrons to escape from implant-induced defects, so that resistivities much higher than those in silicon at room temperature should be possible.

We demonstrate implant isolation of modulation-doped Si 2DEG structures characterized at 4 K. Heavily-doped 2DEGs were used to examine the isolation capability as the worst case scenario (high electron density of ~10^{12} cm^{-2}). Thermal stability was tested for different post-implant annealing temperatures up tp 650 ^{o}C. The 2DEG quality (electron mobility) of samples processed with implant isolation was compared with ones with conventional mesa isolation by reactive ion etching (RIE).

E.2 Sample Growth and Fabrication

The layer structure of the modulation-doped Si 2DEGs used in this study is shown in Fig. E.1. Their Hall mobility, electron density, and sheet resistance at 4 K are in the range of 80,000 to 150,000 cm^2/Vs, 0.8 to 1.6 $\times$ 10^{12} cm^{-2}, and 30 to 80 Ω/□, respectively. The structures were all grown on $Si_{0.7}Ge_{0.3}$ graded buffer substrates by rapid thermal chemical vapor deposition (RTCVD) between 575 ^{o}C and 625 ^{o}C. A test device consists of a set of separated Ohmic contacts to test the implant isolation and a Hall bar structure (in a single 2DEG region) with Ohmic contacts to measure electron mobility and density. After 2DEG growth, a 400-nm masking SiO_2 layer was deposited by plasma-enhanced chemical vapor deposition (PECVD) at 250 ^{o}C. Ohmic contact regions to the 2DEG were then defined by photolithography and diluted HF wet etching of the oxide. 1% Sb-doped Au was thermally evaporated followed by lift-off. Annealing at 450 ^{o}C for 10 min to form Ohmic alloyed contacts was performed before the ion implantation except for samples later annealed at 550 ^{o}C or 650 ^{o}C, where the contacts were formed after 550 ^{o}C or 650 ^{o}C steps. The areas to be isolated were then defined by photolithography and diluted HF wet etching of the oxide.

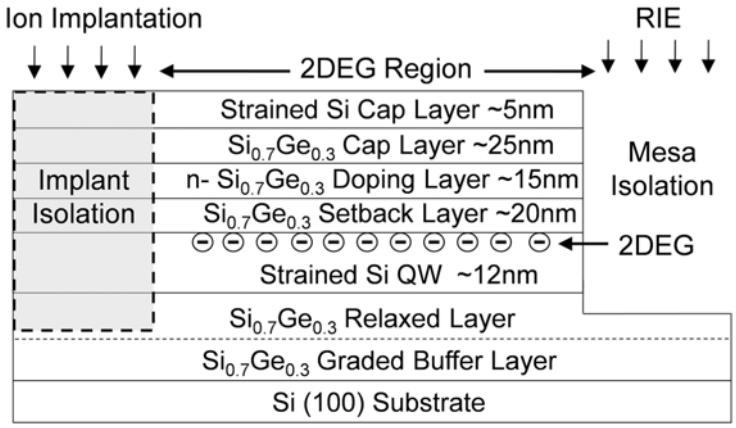

Fig. E.1: The layer structure of a test sample. The layers above the horizontal dotted line were grown by RTCVD. To pattern the 2DEG, only one of implant isolation or conventional mesa isolation by RIE is used on a single sample, but both are illustrated in this figure for brevity.

Isolation tests were done by implanting separately argon (Ar^+) and silicon (Si^+) ions into different samples. Si and Ar were chosen due to their electrical neutrality in the Si/SiGe material system. Two implant energies were used in all regions because both the 2DEG channel and the doping supply layer (if doped above the metal-insulator transition level) [E9] could conduct electricity at low temperature. Therefore, two ion implantation energies of 30 keV and 60 keV were used to create defects near the depth of the shallow doping supply layer (30 keV) and near the deeper strained Si 2DEG channel (60 keV), respectively (Fig. E.2). Silicon amorphized by a high dose implant (~5 $\times$ 10^{14} cm^{-2} for Si^+ into Si at 40 keV) [E11] can be recrystalized by solid phase epitaxy (SPE) at a temperature as low as 500 ^{o}C [E12] (which would lead to poor thermal stability of the damage). Further, SiGe alloys are even more easily amorphized by ion implantation than Si due to weaker bonding between Si and Ge atoms [E13]. Therefore, doses well below 5 $\times$ 10^{14} cm^{-2} were used. Ar^+ or Si^+ was then implanted at room

temperature with three different test doses: 5×10^{11} cm^{-2} (denoted as low dose), 1×10^{13} cm^{-2} (medium dose) and 1×10^{14} cm^{-2} (high dose), and each dose was implanted at two energies, 30 keV and 60 keV. In addition, Hall bars defined by conventional mesa isolation by RIE were also fabricated for 2DEG quality comparison. Ohmic contacts were made on one $Si_{0.7}Ge_{0.3}$ graded buffer substrate separately without implant isolation to test its resistivity at 4 K for reference.

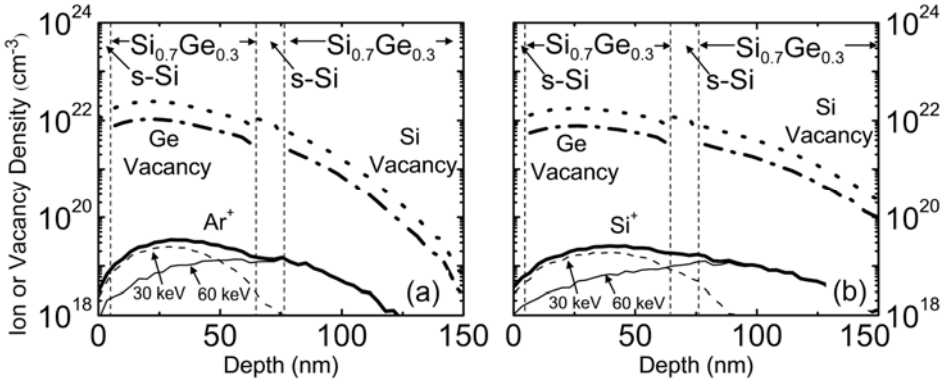

Fig. E.2 Simulation of implanted species and resulting vacancy distribution in a 2DEG structure by the stopping and range of ions in matters (SRIM) software [E10]. Two-step implantation (1×10^{14} cm^{-2}@30 keV+1×10^{14} cm^{-2}@ 60 keV) with implanted species (a) Ar^+ and (b) Si^+ is used in this simulation. The target is assumed to be implanted at 0 K.

E.3 Isolation characterization

The isolation capability at 4 K was examined by two-point measurements between two implant-isolated 2DEGs. Sheet resistances of isolated regions for all six implant conditions are all above $1x10^{12}$ Ω/□, ten orders of magnitude higher than the original 2DEG sheet resistances (Fig. E.3). In some cases, the sheet resistance is as high as $1x10^{13}$ Ω/□, close to the instrumental limit.

Thermal stability issues could arise when we integrate implant isolation technique into a device fabrication process, for example, insulator deposition and contact annealing. Aluminum oxide deposited by atomic layer deposition (ALD) is a common insulator used on enhancement-mode Si 2DEG devices due to its high quality and low deposition temperature (≤ 300 °C) [E14]. To test the thermal stability at the oxide deposition temperature, samples were annealed at 300 °C for 1 h and their sheet resistances were measured at 4 K (Fig. E.3). For samples implanted with medium and high dose, sheet resistances stay high at ~1×10^{13} Ω/□ regardless of implant species, while for ones implanted with a low dose, the sheet resistances drop to 3×10^{10} Ω/□ and 3×10^{3} Ω/□ for Ar^+ and Si^+ implant respectively. Since implantation with the lowest dose (1×10^{11} cm^{-2}) produces the fewer defects (mostly point defects), the damage is easy to anneal and the sheet resistance to decrease. In addition, the higher sheet resistance of low dose Ar^+-implanted sample than Si^+-implanted one after 300 °C annealing might be explained by a higher damage level caused by Ar^+ due to its heavier atomic mass.

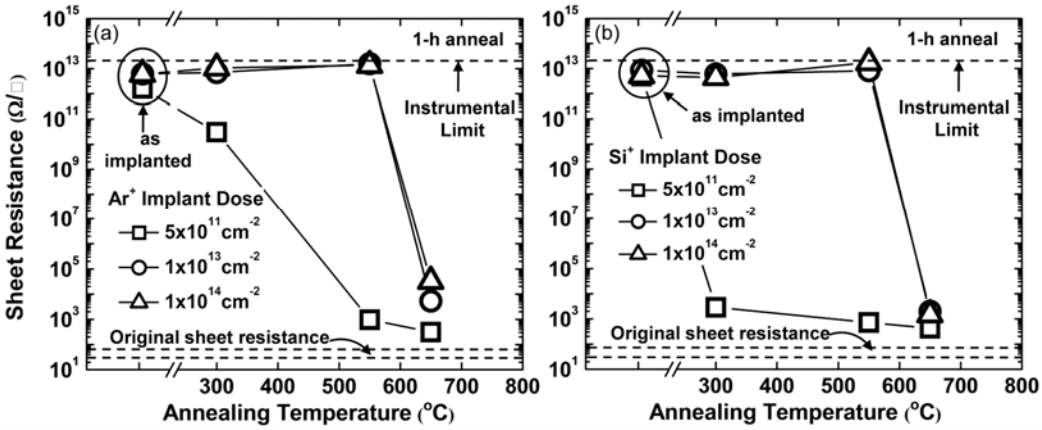

Fig. E.3 Isochronal (1-h) annealing behavior of sheet resistances of 2DEG samples at 4 K implanted with (a) Ar^+ and (b) Si^+ with three various doses, 5×10^{11} cm^{-2}, 1×10^{13} cm^{-2} and 1×10^{14} cm^{-2} at 30 keV and 60 keV. Also shown are the range of sheet resistance of the starting 2DEGs, and the experimental instrumental limitation. The estimated error of sheet resistance is ± 18% for (a) and 27% for (b).

Antimony-doped gold is commonly used on both depletion-mode and enhancement-mode Si/SiGe devices to form Ohmic alloyed contacts after annealing [E14]. However, the necessity of an overlap between the insulated gate and contacts in the enhancement-mode devices for the continuity of conduction makes the requirement of a flat contact surface crucial to prevent possible leakage. Because alloyed contacts have rough surfaces, contacts made by n-type ion implantation are preferred [E4], [E5]. For heavily-phosphorus-implanted contacts, the activation of implanted phosphorus occurs at relatively low temperature (≥ 500 °C) [E12]. Hence, the thermal stability of implant isolation samples was again tested after 550 °C annealing for 1 h. Sheet resistances of the medium and high dose samples at 4 K were $1x10^{13}$ Ω/□ (Fig. E.3) after annealing. After further annealing at 650 °C for 1 h, the sheet resistances of the medium and high dose samples at 4 K drop nine orders of magnitude. Therefore, if an annealing temperature for the contact over 550 °C is desired, it should be done before implant isolation.

Any possible degradation of the 2DEG quality due to spurious radiation during ion implantation was investigated based on Hall mobility measurement by standard low frequency lock-in techniques at 4 K. Fig. E.4 shows the ratio of mobility measured from implant-isolation-defined Hall bars to RIE-defined ones (with absolute mobility values shown in parentheses) from the same CVD growth and annealing condition. Implanted samples without annealing (open symbols) do not show any significant mobility degradation. Even with the highest dose used in this study ($1x10^{14}$ cm^{-2}), the 2DEG quality remains unaffected. Mobility ratios of samples experiencing both implant isolation and 550 °C annealing are also shown in Fig. E.4 (closed symbols). Except for one sample, the mobility ratios after 550 °C annealing are near 100%. We attribute the low mobility ratio for the medium dose Ar^+-implanted sample to a non-uniformity in the 2DEG growth between different wafer pieces used for the Hall bars.

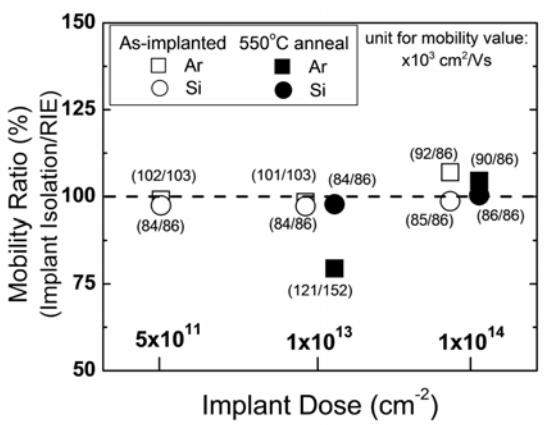

Fig. E.4 Comparison of 2DEG quality after implant isolation or RIE process by the ratio of the mobility at 4 K measured from an implant-isolation-defined Hall bar to a RIE-defined Hall bar for a given implant and anneal. The absolute mobility values at 4 K with a unit of 10^3 cm^2/Vs are shown in parentheses with the mobility for implant isolation before the mobility for mesa isolation. The estimated error of mobility measurement is ± 5%.

F. Topological quantum computing and discovery of Majorana Fermions

F.1 Introduction

All particles are divided into a few fundamental classes depending on how their quantum state evolves upon the exchange of two particles. For non-degenerate states particles exchange results in a wavefunction multiplication by a phase factor, $\psi_f=e^{i\theta}\psi_i$, where quantum statistics in 3D is limited to $\theta=\pi$ (fermions) and $\theta=2\pi$ (bosons). 2D allows existence of particles with fractional statistics (anyons). If particles are *n*-times degenerate, particle exchange is a complex rotation in the *n*-particle space $\psi_f=R\psi_i$ where *R* is $n\times n$ matrix. In general matrices are non-Abelian (matrix multiplication does not commute, $R_1R_2\neq R_2R_1$) thus the wavefunction retains information about topological deformation of the miltiparticle system. This property is at the heart of the topological quantum computing proposal (Kitaev, 2003) [F1], where operations are exchanges of particles with non-Abelian statistics. TQC is inherently fault-tolerant, since all operations can be performed within the ground state of the system and all excitations can be gapped. Despite a number of theoretical works predicting existence of non-Abelian excitations in several exotic systems (p-wave superconductors, 1D organic superconductors, surface of ^{3}He, ν=5/2 FQHE) no experiment demonstrated existence of non-Abelian excitations.

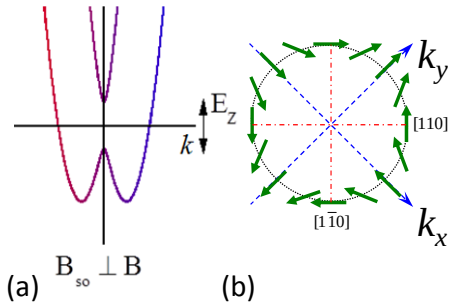

Figure F.1: (a) Lifting of Kramer's degeneracy in 1D system with strong spin-orbit interaction by magnetic field. (b) Symmetry of SO interaction in a 2D (001) InSb electron gas.

F.2 Demonstration of the fractional Josephson effect in 1D InSb/Nb wires

Following theoretical works of Kitaev [F2] and Sau and Alicea [F3,F4] we designed a new system where we measured fractional Josephson effect, the first experimental signature of non-Abelian Majorana fermion excitations [F5]. The system is a 1D wire with strong spin-orbit interaction couples to s-wave superconductor, where Kramer's degeneracy is lifted by magnetic field (Fig. F.1a). In order to realize a topological superconductor with Majorana fermions several conditions should be met: Zeeman splitting E_Z should open a gap large enough for a Fermi level E_F to reside within the gap, $E_Z > \sqrt{\Delta^2 + E_F^2}$ and spin-orbit interaction should be of the order of Zeeman splitting ($E_Z \sim E_{SO}$) to stabilize the proximity-induced superconductivity with the gap Δ. The crystalline Dresselhause SO interaction is cubic in k in bulk III-V semiconductors and become linear in thin quantum wells, $E_{SO} = \sqrt{2}\gamma_D\langle k_z^2\rangle k = \sqrt{2}\gamma_D(\pi/d)^2 k$, where d is the width of the well. We fabricated our samples from a 20-nm thick InSb layer. The symmetry of SO effective field is shown in Fig. F.1b. Heterostructure material is grown in the laboratory of Profs. X. Liu and J. Furdyna at University of Notre Dame and consist of a 20nm relaxed 20-nm InSb layer grown on a 1.2 μm-thick graded In_xGa_{1-x} Sb buffer over a GaSb substrate.

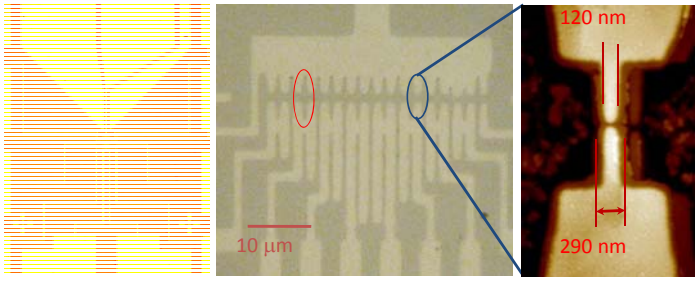

Figure F.2: Optical micrograph of a device and an AFM micrograph of a Josephson junction region.

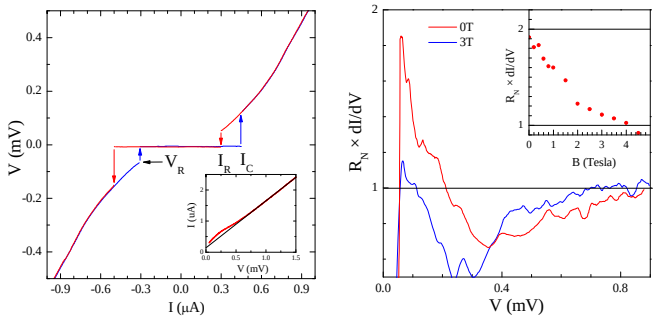

Figure F.3: I/V characteristic of a JJ. Excess current at low biases is due to Andreev reflection, this coherent transport is observed for B up to 4 Tesla.

In our experiments Nb/InSb/Nb Josephson junctions (JJs) are fabricated lithographically from a shallow InSb quantum well. Superconductivity in InSb is induced by the proximity effect from a Nb film placed on top of the InSb nanowire. We developed a self-aligning fabrication process where a single step e-beam lithography is used to fabricate a JJ and a continuous InSb wire beneath the junction. A pattern of multiple JJs is defined by e-beam lithography, and a 45 nm layer of Nb is deposited by dc sputtering on top of the InSb quantum well. A sample outline and an AFM micrograph of an individual junction is shown in Fig. 2. A weak link is formed between two 120 nm-wide and 0.6 μm-long Nb wires, with gaps ranging from 20 to 120 nm in different devices. The InSb wires have a rectangular cross section ~250 nm × 20 nm oriented along [110] crystallographic axis, we estimate the strength of SO interaction in our samples $E_{SO} \approx 2.6 \cdot 10^{-6} k$ [meV cm], some 20 time stronger than in CVD-grown InSb wires. We also

estimate that several (3-7) one-dimensional subbands are occupied in our devices. The JJ have T_C~1K, factor of 2 reduction from the T_C in the adjacent Nb wires (in wide Nb regions we have T_C>7K). Nb wires are type-II superconductors with B_{C1}=2.5T and B_{C2}=5T. A typical I/V characteristic of a JJ shows moderate hysteresis, Fig. F.3, and current enhancement due to Andreev reflection at low biases is observed in fields up to 4 Tesla. Coherent transport, which leads to the current enhancement, is required for the formation of coherent Majorana bound states.

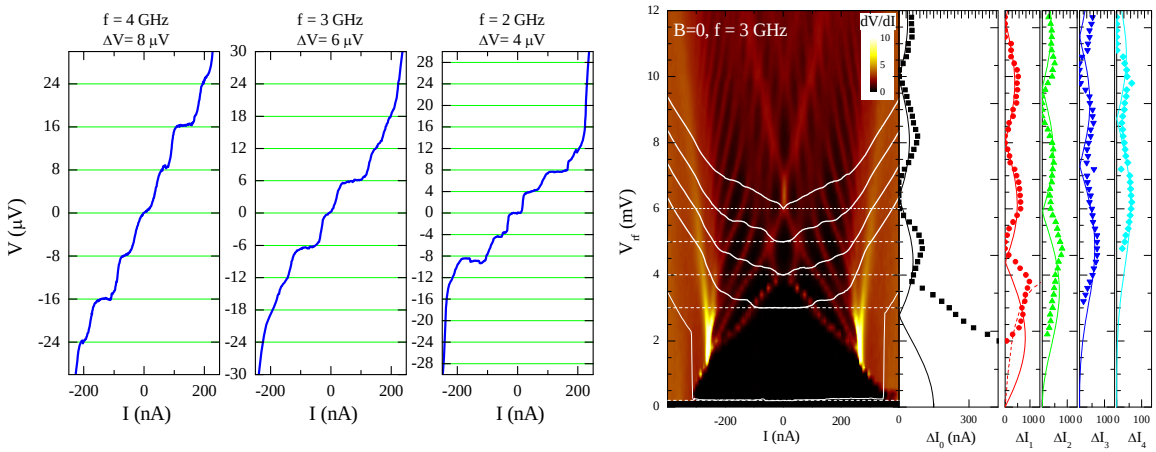

Figure F.4: I/V characteristic of a JJ irradiated by rf. Color plot is differential resistance plotted as a function of rf power, where black regions correspond to the Shapiro steps. Shapiro step width follows expected Bessel function dependence as a function of rf power.

RF wiring of the dilution refrigerator, developed during the Phase-I of the project, was crucial to the success of these experiments. In Figure F.4 we show I/V characteristic of the JJ at B=0 when junction is irradiated with rf frequency 2, 3 and 4 GHz. Voltage steps with the height $\frac{\hbar\omega_{rf}}{2e} = 4$, 6 and 8 μV respectively are clearly observed, so-called Shapiro steps. The height of the step corresponds to 2e charge transfer per photon. Power dependence of Shapiro steps follows an expected Bessel function dependence.

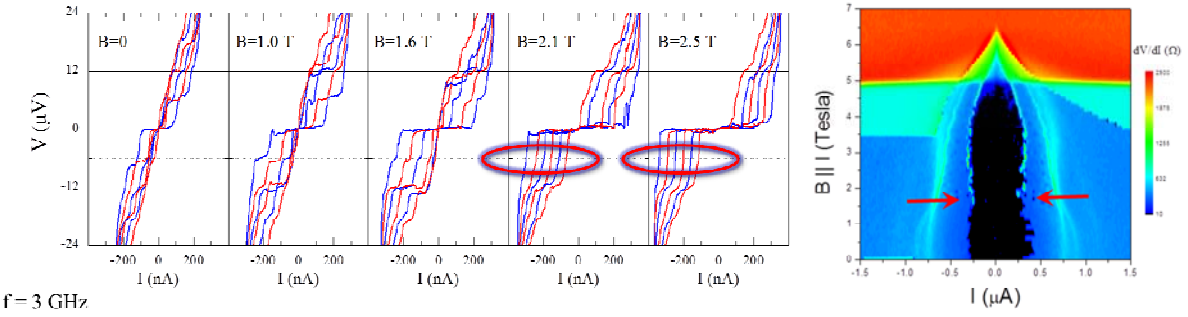

Figure F.5: Shapiro steps at different magnetic fields. Steps with 6 μV (2e charge transfer) are observed for B<2T, while steps are doubled (charge 1e transfer) for B>2T. Right plot: suppression of critical current at B=2 T is clearly observed in differential resistance.

As magnetic field is applied, the wires undergo a topological phase transition around B=2T, where the height of the Shapiro step doubles, see Figure F.5. The step at V = 6 μV is prominently observed at B<2 Tesla, while the first step has twice the height, V = 12 μV, at B>2 Tesla. Doubling of the Shapiro step height is a unique signature of Majorana fermions formation, where fusion of Majorana fermions results in a charge 1e transfer per photon, or step height —— V. At the field where topological transition takes place superconducting gap should collapse. In our experiments we do not measure the gap directly. Critical current, measured in our experiments, is not expected to vanish at the transition because the density of gapped (Cooper pair) excitations is larger than the density of non-gapped ones (Majorana fermions). Instead, we observe suppression of the critical current near the topological phase transition, see Fig F.6.

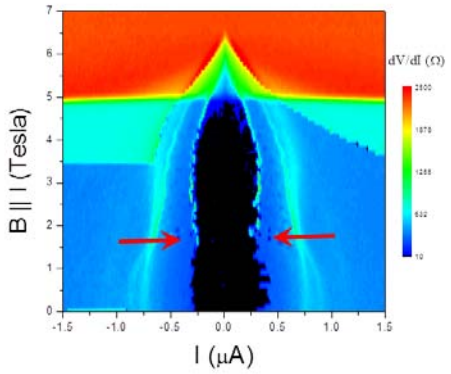

Figure F.6. Suppression of the critical current at the topological phase transition (B=2 Tesla)

Short of particle braiding and demonstration of non-Abelian statistics, this work is the most direct observation of Majorana fermions up today. The work was featured at Nature News & Views [NP **8**, 778 2012] and various media publications. The next major step toward development of a topological fault-tolerant quantum computer will be development of a system where Majorana fermions can be manipulated in 2D and multi-particle braiding can be demonstrated.

5. Bibliography

[A1] T. Ando, A. B. Fowler, and F. Stern, "Electronic properties of two-dimensional system," *Review of Modern Physics*, vol. 54, pp. 437 – 672, 1982.

[A2] K. Klitzing, G. Dorda, and M. Pepper, "New method for high-accuracy determination of the fine-Structure constant based on quantized Hall resistance," *Physical Review Letters*, vol. 45, pp. 494 – 497, 1980.

[A3] D. C. Tsui, H. L. Störmer, A. C. Gossard, "Two-dimensional magnetotransport in the extreme quantum limit," *Physical Review Letters*, vol. 48, pp. 1559 – 1562, 1982.

[A4] K. Ismail, J. O. Chu, and M. Arafa, "Integrated enhancement- and depletion-mode FET's in modulation-doped Si/SiGe heterostructures," *IEEE Electron Device Letters*, vol. 18, pp. 435 – 437, 1997.

[A5] N. A. Gershenfeld and I. L. Chuang, "Bulk spin-resonance quantum computation," *Science*, vol. 275, pp. 350 – 356, 1997.

[A6] R. Dingle, H. L. Störmer, A. C. Gossard, "Electron mobilities in modulation-doped semiconductor heterojunctions superlattices," *Applied Physics Letters*, vol. 33, pp. 665 – 667, 1978.

[A7] V. Umansky, M. Heiblum, Y. Levinson, J. Smet, J.Nübler, and M. Dolev, " MBE growth of ultra-low disorder 2DEG with mobility exceeding 35 $\times$ 10^6 cm^2/Vs," *Journal of Crystal Growth*, vol. 311, pp. 1658 – 1661, 2009.

[A8] G. Abstreiter, H. Brugger, T. Wolf, H. Jorke, and H. J. Herzog, "Strained-induced two-dimensional electron gas in selectively doped Si/Si_xGe_{1-x} superlattices," *Physical Review Letters*, vol. 54, pp. 2441 – 2444, 1985.

[A9] K. Ismail, M. Arafa, K. L. Saenger, J. O. Chu, and B. S. Meyerson, "Extremely high electron mobility in Si/SiGe modulation-doped heterostructures," *Applied Physics Letters*, vol. 66, pp. 1077 – 1079, 1995.

[A10] N. Sugii, K. Nakagawa, Y. Kimura, S. Yamaguchi, and M. Miyao, "High electron mobility in strained Si channel of $Si_{1-x}Ge_x/Si/Si_{1-x}Ge_x$ heterostructure with abrupt interface," *Semiconductor Science and Technology*, vol. 13, pp. A140 – A142, 1998.

[A11] S. -H. Huang, T. -M. Lu, S. -C. Lu, C. -H. Lee, C. W. Liu, and D. C. Tsui, "Mobility enhancement of strained Si by optimized SiGe/Si/SiGe structures," *Applied Physics Letters*, vol. 101, p. 042111, 2012.

[A12] E. Kasper and K. Lyutovich, *Properties of Silicon Germanium and SiGe:Carbon*, INSPEC, 2000.

[A13] D. J. Paul, "Si/SiGe heterostructures: from material and physics to devices and circuits," *Semiconductor Science and Technology*, vol. 19, pp. R75 – R108, 2004.

[A14] E. Kasper and K. Lyutovich, *Properties of Silicon Germanium and SiGe:Carbon*, INSPEC, 2000.

[A15] G. P. Watson, E. A. Fitzgerald, Y. -H. Xie, and D. Monroe, "Relaxed low threading defect density $Si_{0.7}Ge_{0.3}$ epitaxial layers grown on Si by rapid thermal chemical vapor deposition," *Journal of Applied Physics*, vol. 75, pp. 263 – 269, 1994.

[A15] Y. Sun, Z. Liu, S. Sun, and P. Pianetta, "The effectiveness of HCl and HF cleaning of $Si_{0.85}Ge_{0.15}$ surface," *Journal of Vacuum Science and Technology A*, vol. 26, pp. 1248 – 1250, 2008.

[A16] D. J. Paul, A. Ahmed, M. Pepper, A. C. Churchill, D. J. Robbins, D. J. Wallis, and A. J. Pidduck, "Electrical properties and uniformity of two dimensional electron gases grown on cleaned SiGe virtual substrates," *Journal of Vacuum Science and Technology B*, vol. 16, pp. 1644 – 1647, 1998.

[A17] 1D Poisson solver by G. Snider: http://www3.nd.edu/~gsnider/

[A18] J. H. Davies, *The Physics of Low-Dimensional Semiconductors*, Cambridge, 1998.

[A19] R. People and J. C. Bean, "Band alignments of coherently strained Ge_xSi_{1-x}/Si heterostructures on <001> Ge_ySi_{1-y} substrates," *Applied Physics Letters*, vol. 48, pp. 538 – 540, 1986.

[A20] D. Monroe, Y. -H. Xie, E. A. Fitzgerald, P. J. Silverman, and G. P. Watson, "Comparison of mobility-limiting mechanisms in high-mobility $Si_{1-x}Ge_x$ heterostructures," *Journal of Vacuum Science and Technology B*, vol. 11, pp. 1731 – 1737, 1993.

[A21] G. I. Ritter, B. Tillack, and D. Wolansky, "Memory effect in RTCVD epitaxy of Si and SiGe," *MRS Proceedings*, vol. 429, pp. 379 – 384, 1996.

[A22] J. Y. Li, C. T. Huang, L. P. Rokhinson, and J. C. Sturm, "Extremely low electron density in a modulation-doped Si/SiGe two-dimensional electron gases by effective Schottky gating," *ECS Transactions*, vol. 50, pp. 145 – 149, 2012.

[A23] C. A. Richter, R. G. Wheele, and R. N. Sacks, "Overshoots of quantum Hall plateaus," *Surface Science*, vol. 263, pp. 270 – 274, 1992.

[A24] S. Komiyama, H. Nii, M. Ohsaw, S. Fukatsu, Y. Shiraki, R. Itoh, and H. Toyoshima, "Resistance and resistivity of two dimensional electron gas at high magnetic fields," *Solid State Communications*, vol. 80, pp. 157 – 163, 1991.

[A25] J. W. Matthews and A. E. Blakeslee, "Defects in epitaxial multilayers: I. Misfit dislocations," *Journal of Crystal Growth*, vol. 27, pp. 118 – 125, 1974.

[B1] J. R. Petta, A. C. Johnson, J. M. Taylor, E. A. Laird, A. Yacoby, M. D. Lukin, C. M. Marcus, M. P. Hanson, and A. C. Gossard, "Coherent manipulation of coupled electron spins in semiconductor quantum dots," *Science*, vol. 309, pp. 2180 – 2184, 2005.

[B2] B. M. Maune1, M. G. Borselli1, B. Huang, T. D. Ladd, P. W. Deelman, K. S. Holabird, A. A. Kiselev, I. Alvarado-Rodriguez, R. S. Ross, A. E. Schmitz, M. Sokolich, C. A. Watson, M. F. Gyure, and A. T. Hunter, "Coherent singlet-triplet oscillations in a silicon-based double quantum dot," *Science*, vol. 481, pp. 344 – 347, 2012.

[B3] D. R. Lide, *CRC Handbook of Chemistry and Physics*, CRC Press, 2006.

[B4] A. Wild, J. Kierig, J. Sailer, J. W. Ager III, E. E. Haller, G. Abstreiter, S. Ludwig, and D. Bougeard, "Few electron double quantum dot in an isotopically purified ^{28}Si quantum well," *Applied Physics Letters*, vol. 100, p. 143110, 2012.

[B5] L. V. C. Assali, H. M. Petrilli, R. B. Capaz, B. Koiller, X. Hu, and S. Das Sarma, "Hyperfine interactions in silicon quantum dots," *Physical Review B*, vol. 83, p. 165301, 2011.

[B6] A. C. Johnson, J. R. Petta, J. M. Taylor, A. Yacoby, M. D. Lukin, C. M. Marcus, M. P. Hanson, and A. C. Gossard, "Triplet-singlet spin relaxation via nuclei in a double quantum dot," *Nature*, vol. 435, pp. 925 – 928, 2005.

[B7] J. A. Nixon and J. H. Davies, "Potential fluctuations in heterostructure devices," Physical Review B, vol. 41, pp. 7929 – 7932, 1990.

[B8] D. Laroche, S. Das Sarma, G. Gervais, M. P. Lilly, and J. L. Reno, "Scattering mechanism in modulated-doped shallow two-dimensional electron gas," *Applied Physics Letters*, vol. 96, p. 162112, 2010.

[C1] C. Payette, K. Wang, P. J. Koppinen, Y. Dovzhenko, J. C. Sturm, and J. R. Petta, "Single charge sensing and transport in double quantum dots fabricated from commercially grown Si/SiGe heterostructures," *Applied Physics Letters*, vol. 100, p. 043508, 2012.

[C2] D. V. Yurasov, M. N. Drozdov, A. V. Murel, M. V. Shaleev, N. D. Zakharov, and A. V. Novikov, "Usage of antimony segregation for selective doping of Si in molecular beam epitaxy," *Journal of Applied Physics*, vol. 109, p. 113533, 2011.

[C3] K. D. Hobart, F. J. Kub, G. G. Jernigan, and P. E. Thompson, "Surface segregation of arsenic and phosphorus from buried layers during Si molecular beam epitaxy," *Journal of Vacuum Science and Technology B*, vol. 14, pp. 2229 – 2232, 1996.

[C4] M. Yang, M. Carroll, J. C. Sturm, and T. Büyüklimanli, "Phosphorus doping and sharp profiles in silicon and silicon-germanium epitaxy by rapid thermal chemical vapor deposition," *Journal of the Electrochemical Society*, vol. 147, pp. 3541 – 3545, 2000.

[C5] D. V. Singh, J. L. Hoyt, and J. F. Gibbons, "Abrupt phosphorus profiles in Si: Effects of temperature and substitutional carbon on phosphorus autodoping," *Journal of Electrochemical Society*, vol. 150, pp. G553 – G556, 2003.

[C6] J.Tersoff, "Carbon defects and defect reactions in silicon," *Physical Review Letters*, vol. 64, pp. 1757 – 1760, 1990.

[C7] J. F. Nützel and G. Abstreiter, "Comparison of P and Sb as n-dopants for Si molecular beam epitaxy," *Journal of Applied Physics*, vol. 78, pp. 937 – 940, 1995.

[C8] J. J. Harris, D. E. Ashenford, C. T. Foxon, P. J. Dobson, and B. A. Joyce, "Kinetic limitations to surface segregation during MBE growth of III-V compounds: Sn in GaAs," *Applied Physics A*, vol. 33, pp. 87 – 92, 1984.

[C9] B. Cho, J. Bareño, Y. L. Foo, S. Hong, T. Spila, I. Petrov, and J. E. Greene, "Phosphorus incorporation during Si (001):P gas-source molecular beam epitaxy: Effects on growth kinetics and surface morphology," *Journal of Applied Physics*, vol. 103, p. 123530, 2008.

[C10] M. L. Yu, D. J. Vitkavage, and B. S. Meyerson, "Doping reaction of PH_3 and B_2H_6 with Si(100)," *Journal of Applied Physics*, vol. 59, pp. 4032 – 4037, 1986.

[C11] P. Sen, B. C. Gupta, and I. P. Batra, "Structures studies of phosphorus induced dimers on Si(001)," *Physical Review B*, vol. 73, p. 085319, 2006.

[C12] J. F. Nützel, M. Holzmann, P. Schittenhelm, and G. Abstreiter, "Segregation of n-dopants on SiGe surfaces," *Applied Surface Science*, vol. 102, pp. 98 – 101, 1996.

[C13] M. -H. Xie, A. K. Lees, J. M. Fernandez, J. Zhang, and B. A. Joyce, "Arsenic surface segregation and incorporation in Si and $Si_{1-x}Ge_x$ during gas source molecular beam epitaxy," *Journal of Crystal Growth*, vol. 173, pp. 336 – 342, 1997.

[C14] M. -H. Xie, J. Zhang, A. Lees, J. M. Fernandez, and B. A. Joyce, "Surface segregation during molecular beam epitaxy: the site-blocking effects of surfactant atoms," *Surface Science*, vol. 367, pp. 231 – 237, 1996.

[C15] H. Kim, N. Taylor, J. R. Abelson, and J. E. Greene, "Effects of H coverage on Ge segregation during $Si_{1-x}Ge_x$ gas-source molecular beam epitaxy," *Journal of Applied Physics*, vol. 82, pp. 6062 – 6066, 1997.

[C16] J. Y. Li, C. T. Huang, J. C. Sturm, "The effect of hydrogen on the surface segregation of phosphorus in epitaxially grown relaxed $Si_{0.7}Ge_{0.3}$ films by rapid thermal chemical vapor deposition," *Applied Physics Letters*, vol. 101, p. 142112, 2012.

[C17] L. Oberbeck, N. J. Curson, T. Hallam, M. Y. Simmons, G. Bilger, and R. G. Clark, "Measurement of phosphorus segregation in silicon at the atomic scale using scanning tunneling microscopy," *Applied Physics Letters*, vol. 85, pp. 1359 – 1361, 2004.

[C18] J. F. Nützel and G. Abstreiter, "Segregation and diffusion on semiconductor surfaces," *Physical Review B*, vol. 53, pp. 13551 – 13558, 1996.

[C19] E. S. Tok, S. W. Ong, and H. Chuan Kang, "Hydrogen desorption kinetics from the $Si_{1-x}Ge_x$(100)–(2 $\times$1) surface," *Journal of Chemical Physics*, vol. 120, 5424 – 5431, 2004.

[C20] D. A. Grützmacher, T. O. Sedgwick, A. Powell, M. Tejwani, S. S. lyer, J. Cotte, and F. Cardone, "Ge segregation in SiGe/Si heterostructures and its dependence on deposition technique and growth atmosphere," *Applied Physics Letters*, vol. 63, pp. 2531 – 2533, 1993.

[C21] M. J. -P. Duchemin, M. M. Bonnet, and M. F. Koelsch, "Kinetics of silicon growth under low hydrogen pressure," *Journal of the Electrochemical Society*, vol. 125, pp. 637 – 644, 1978.

[D1] K. Yao, *Silicon and Silicon-Germanium Epitaxy for Quantum Dot Device Fabrications towards an Electron Spin-Based Quantum Computer*, Ph.D. dissertation, Princeton University, 2009.

[D2] M. Kellogg, J. P. Eisenstein, L. N. Pfeiffer, and K. W. West, "Vanishing Hall resistance at high magnetic field in a double-layer two-dimensional electron system," *Physical Review Letters*, vol. 93, p. 036801, 2004.

[D3] D.J. Paul, A. Ahmed, A.C. Churchill, D.J. Robbins, and W.Y. Leong, "Low-dimensional inverted Si/SiGe modulation-doped electron gases using selective ex-situ ion implantation," *Materials Science and Engineering B*, vol. 89, pp. 111 – 115, 2002.

[D4] A. Gold, "Mobility and metal–insulator transition of the two-dimensional electron gas in SiGe/Si/SiGe quantum wells," *Journal of Applied Physics*, vol. 108, p. 063710, 2010.

[D5] H. Sakaki, T. Noda, K. Hirakawa, M. Tanaka, and T. Matsusue, "Interface roughness scattering in GaAsl/AlAs quantum wens," *Applied Physics Letters*, vol. 51, pp. 1934 – 1936, 1987.

[D6] M. A. Reed, W. P. Kirk, and P. S. Kobiela, "Investigating of parallel conduction in GaAs/$Al_xGa_{1-x}As$ modulation-doped structures in the quantum limit," *IEEE Journal of Quantum Electronics*, vol. 22, pp. 1753 – 1759, 1986.

[D7] K. Ensslin, D. Heitmann, R. R. Gerhardts, and K. Ploog, "Population process of the upper subband in $Al_xGa_{1-x}As$-GaAs quantum wells," *Physical Review B*, vol. 39, pp. 12993 – 12996, 1989.

[D8] H. L. Stömer, A. C. Gossard, and W. Wiegmann, "Observation of intersubband scattering in a 2-dimensional electron system," *Solid State Communications*, vol. 41, pp. 707 – 709, 1982.

[D9] T. P. Smith III and F. F. Fang, "Upper-subband transport in GaAs heterostructures," *Physical Review B*, vol. 37, pp. 4303 – 4305, 1988.

[D10] R. Fletcher, E. Zaremba, M. D'Iorio, C. T. Foxon, and J. J. Haris, "Evidence of a mobility edge in the second subband of an $Al_{0.33}Ga_{0.67}As$-GaAs heterojunctions," *Physical Review B*, vol. 38, pp. 7866 – 7869, 1988.

[E1] R. Hanson et al., "Spins in few-electron quantum dots," *Rev. Mod. Phys.,* vol.79, pp. 1217-1265, Oct. 2007.

[E2] A. M. Tyryshkin, S. A. Lyon, A. V. Astashkin, and A. M. Raitsimring, "Electron spin relaxation times of phosphorus donors in silicon," *Phys. Rev. B,* vol. 68, pp. 193207, Nov. 2003.

[E3] T. Berer et al., "Lateral quantum dots in Si/SiGe realized by a Schottky split-gate technique," *Appl. Phys. Lett.,* vol.88, pp. 162112, Apr. 2006.

[E4] T. M. Lu et al., "Enhancement-mode buried strained silicon channel quantum dot with tunable lateral geometry," *Appl. Phys. Lett.,* vol. 99, pp. 043101, Jul. 2011.

[E5] B. M. Maune et al., "Coherent singlet-triplet oscillations in a silicon-based double quantum dot," *Nature,* vol. 481, pp. 344-347, Nov. 2011.

[E6] S. J. Pearton, "Ion implantation for isolation of III-V semiconductors," *Mater. Sci. Rep.,* Vol.4, pp. 313-363, Oct. 1989.

[E7] J. A. Yasaitis, "Ion implantation of Neon in silicon for planar amorphous isolation," *Electron. Lett.,* vol. 14, no.15, pp. 460-461, Jun. 1978

[E8] T.M. Lu et al., "Process development toward enhancement-mode strained-Si/SiGe double quantum dot," in *Proc. ISTDM*, 2012, pp.180-181

[E9] C. Yamanouchi, K. Mizuguchi and W. Sasaki, "Electric conduction in phosphorus doped silicon at low temperature," *J. Phys. Soc. Jpn.*, vol. 22, no. 3, Mar. 1967.

[E10] J. F. Ziegler, J. P. Biersack and L. Haggmark, (2012), The Stopping and Ranges of Ion s in Matters. Available: www.srim.org.

[E11] J. F. Gibbons, "Ion implantation in semiconductors-Part II: damage production and annealing," *Proc. IEEE*, vol. 60, pp.1062-1096, Sep, 1972.

[E12] S. A. Campbell, *Fabrication engineering at the micro-and nanoscale. 3rd ed.,* New York, Oxiford University Press, 2008, pp.124-125.

[E13] A. N. Larsen et al., "MeV ion implantation induced damage in relaxed Si1-xGex," *J. Appl. Phys.,* vol. 81, no. 5, pp. 2208-2218, Mar. 1997

[E14] T. M. Lu, D. C. Tsui, C. –H. Lee, and C. W. Liu, "Observation of two-dimensional electron gas in a Si quantum well with mobility of 1.6x106 cm2/Vs," *Appl. Phys. Lett.,* vol. 94, pp. 182102, May 2009.

[F1] Kitaev, A. Y. Fault-tolerant quantum computation by anyons. Ann. Phys. **303**, 2–30 (2003)
[F2] Kitaev, A. Y. Unpaired Majorana fermions in quantum wires. Phys.-Usp. **44**, 131–136 (2001)
[F3] Sau, J., Lutchyn, R., Tewari, S. & Das Sarma, S. Generic new platform for topological quantum computation using semiconductor heterostructures. Phys. Rev. Lett. **104**, 040502 (2010)
[F4] Alicea, J., Oreg, Y., Refael, G., von Oppen, F. & Fisher, M. P. A. Non-Abelian statistics and topological quantum information processing in 1D wire networks. Nature Phys. **7**, 412–417 (2011)
[F5] L. P. Rokhinson, X. Liu, J. K. Furdyna, Observation of the fractional ac Josephson effect: the signature of Majorana particles, Nature Physics **8**, 795 (2012)

6. Appendix

The following two manuscripts under preparation are based on the work supported by this grant and will be submitted soon:

[1] J. Y. Li, C. T. Huang, L. P. Rokhinson, and J. C. Sturm, "Extremely high electron mobility in an inverted modulation-doped Si two-dimensional electron gas by a sharp turn-off of phosphorus," manuscript in preparation.

[2] J. Y. Li, C. T. Huang, L. P. Rokhinson, and J. C. Sturm, "Extremely high electron mobility in isotopically enriched ^{28}Si quantum wells grown by chemical vapor deposition," manuscript to be submitted to *Applied Physics Letters*.